Article

Developmental Cell

An Orchestrated Intron Retention Program in Meiosis Controls Timely Usage of Transcripts during Germ Cell Differentiation

Highlights

- Alternative splicing in meiotic spermatocytes favors intron retention
- Intron retention stabilizes nuclear transcripts in meiotic spermatocytes
- A high transcription rate outcompetes the spliceosome from weak introns in meiosis
- Long-lived intron-retaining mRNAs encode key proteins for male gamete function

Authors

Chiara Naro, Ariane Jolly, Sara Di Persio, ..., Raffaele Geremia, Pierre De la Grange, Claudio Sette

Correspondence

claudio.sette@uniroma2.it

In Brief

Transcription during mammalian spermatogenesis is discontinuous and ceases in late post-meiotic stages. Naro et al. show that regulated intron retention in male meiotic germ cells generates long-lived intron-retaining transcripts that are preserved for days after their synthesis and can be timely translated by transcriptionally inactive post-meiotic germ cells.

Naro et al., 2017, Developmental Cell *41*, 1–12
April 10, 2017
http://dx.doi.org/10.1016/j.devcel.2017.03.003

CellPress

Please cite this article in press as: Naro et al., An Orchestrated Intron Retention Program in Meiosis Controls Timely Usage of Transcripts during Germ Cell Differentiation, Developmental Cell (2017), http://dx.doi.org/10.1016/j.devcel.2017.03.003

Developmental Cell
Article

An Orchestrated Intron Retention Program in Meiosis Controls Timely Usage of Transcripts during Germ Cell Differentiation

Chiara Naro,[1,2] Ariane Jolly,[3] Sara Di Persio,[4] Pamela Bielli,[1,2] Niclas Setterblad,[5] Antonio J. Alberdi,[5] Elena Vicini,[4] Raffaele Geremia,[1] Pierre De la Grange,[3] and Claudio Sette[1,2,6,*]

[1]Department of Biomedicine and Prevention, University of Rome Tor Vergata, Via Montpellier 1, 00133 Rome, Italy
[2]Laboratories of Neuroembryology, Fondazione Santa Lucia IRCCS, 00143 Rome, Italy
[3]GenoSplice Technology, iPEPS-ICM, Hôpital de la Pitié Salpêtrière, 75013 Paris, France
[4]Fondazione Pasteur Cenci Bolognetti, Department of Anatomy, Histology, Forensic Medicine and Orthopedic, Section of Histology Sapienza University of Rome, 00161 Rome, Italy
[5]IUH, Saint-Louis Hospital, 75010 Paris, France
[6]Lead Contact
*Correspondence: claudio.sette@uniroma2.it
http://dx.doi.org/10.1016/j.devcel.2017.03.003

SUMMARY

Global transcriptome reprogramming during spermatogenesis ensures timely expression of factors in each phase of male germ cell differentiation. Spermatocytes and spermatids require particularly extensive reprogramming of gene expression to switch from mitosis to meiosis and to support gamete morphogenesis. Here, we uncovered an extensive alternative splicing program during this transmeiotic differentiation. Notably, intron retention was largely the most enriched pattern, with spermatocytes showing generally higher levels of retention compared with spermatids. Retained introns are characterized by weak splice sites and are enriched in genes with strong relevance for gamete function. Meiotic intron-retaining transcripts (IRTs) were exclusively localized in the nucleus. However, differently from other developmentally regulated IRTs, they are stable RNAs, showing longer half-life than properly spliced transcripts. Strikingly, fate-mapping experiments revealed that IRTs are recruited onto polyribosomes days after synthesis. These studies reveal an unexpected function for regulated intron retention in modulation of the timely expression of select transcripts during spermatogenesis.

INTRODUCTION

Spermatogenesis is a remarkable cell differentiation process that yields the male gamete and remains active throughout the adult life of mammals (Griswold, 2016). It comprises three main phases: a "mitotic" phase during which spermatogonia stem cells divide either to self-renew or to originate successive generations of mitotic spermatogonial cells; a "meiotic" phase during which primary spermatocytes engage two consecutive divisions that increase genetic variability and half genome content; and "spermiogenesis" when haploid spermatids undergo dramatic morphological changes, such as DNA compaction and development of a motile flagellum, which endow the mature spermatozoa with features essential for fertilization (Hermo et al., 2010a, 2010b).

Each stage of spermatogenesis requires a specific repertoire of factors to accomplish the profound genomic and morphological modifications that characterize male germ cell differentiation. Proper expression of these factors is dynamically controlled at transcriptional and post-transcriptional levels (Paronetto and Sette, 2010; Chalmel and Rolland, 2015). Testicular paralogs of core transcriptional components, such as TAF7L (Zhou et al., 2013), or testis-specific transcription factors, such as the cyclic AMP-responsive factor CREM (Nantel and Sassone-Corsi, 1996), together with stage-specific epigenetic modifications (Godmann et al., 2007; Soumillon et al., 2013; Hammoud et al., 2014), contribute to orchestrate gene expression programs during spermatogenesis. Moreover, since transcription is not continuously active during male germ cell differentiation (Monesi, 1964), translational regulation of stored mRNAs ensures timely expression of proteins in the transcriptionally silent stages of spermatogenesis (Paronetto and Sette, 2010).

High-throughput transcriptome analyses identified testis among the tissues displaying the highest proportion of splice variants (Kan et al., 2005), with germ cells providing the largest contribution to this transcriptome complexity (Soumillon et al., 2013). Moreover, profiling of whole testis transcriptome during the first wave of mouse spermatogenesis highlighted some alternative splicing (AS) events that are timely regulated during this process (Schmid et al., 2013; Margolin et al., 2014). AS of exons and introns in virtually every mammalian gene yields multiple transcripts that often display different coding properties and/or patterns of spatial/temporal expression (Barbosa-Morais et al., 2012; Yang et al., 2016). In this way, AS represents a powerful resource to amplify the complexity and flexibility of the genome and to precisely modulate gene expression during cell differentiation and development (Kalsotra and Cooper, 2011). Thus, AS modulation likely contributes to fine-tune the germ cell differentiation program.

To date, no study has investigated whether global splicing changes occur during the transmeiotic phases of spermatogenesis, when unique processes take place. Indeed, meiotic

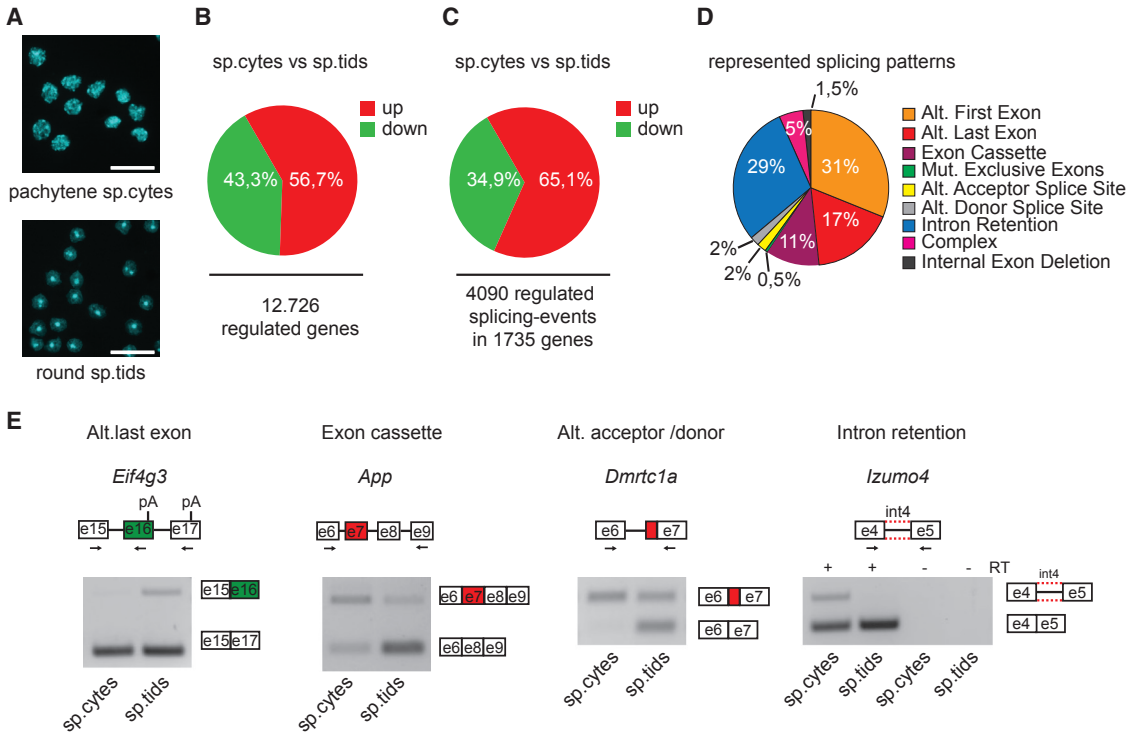

Figure 1. An Extensive Alternative Splicing Program Characterizes the Meiotic Transition of Male Germ Cells

(A) Representative images of Hoechst nuclear staining of purified cellular populations of meiotic pachytene spermatocytes (sp.cytes, upper panel) and post-meiotic round spermatids (sp.tids, lower panel). Scale bar, 25 μm.

(B and C) Pie charts showing percentages of expression-regulated genes (B) and splicing-regulated exons (C) identified in sp.cytes compared with sp.tids (fold change ≥ 2; $p \leq 0.05$).

(D) Pie chart representing distribution of regulated splicing events in sp.cytes versus sp.tids among different splicing patterns.

(E) Representative images of RT-PCR analyses for indicated AS events differentially regulated between sp.cytes and sp.tids. Schematic representation for each event analyzed is depicted above the representative agarose gel. Red and green boxes indicate respectively up- and downregulated events in sp.cytes compared with sp.tids. Black arrows in the scheme indicate primers used for the PCR analysis.

See also Figure S1.

spermatocytes undergo homologous recombination and chromosome segregation, whereas post-meiotic spermatids need to differentiate into highly specialized, motile spermatozoa (Griswold, 2016; Hermo et al., 2010a, 2010b), and all of these events require specific factors that are often only expressed in germ cells. In this study, by performing high-throughput transcriptome profiling of purified male germ cells we uncovered a robust intron retention (IR) program in meiotic spermatocytes. Intron-retaining genes were strongly enriched in functional categories related to differentiation and properties of the male gamete. Mechanistically, we found that weak splice sites coupled with high RNA polymerase II (RNAPII) activity contribute to IR in spermatocytes. Reducing the transcriptional burden by inhibiting RNAPII phosphorylation rescued splicing, suggesting that competition for the spliceosome selects weak introns for retention. Although IR was generally shown to cause transcript instability in mammals, thus contributing to the quenching of gene expression during cell differentiation or in response to stress (Yap et al., 2012; Wong et al., 2013; Shalgi et al., 2014; Edwards et al., 2016; Pimentel et al., 2016; Ni et al., 2016), we found that meiotic intron-retaining transcripts (IRTs) are long-lived mRNAs, which are preserved until they need to be translated. Thus, our study reveals an unexpected physiological role for IR in ensuring proper and timely control of gene expression during male germ cell differentiation.

RESULTS

A Regulated Alternative Splicing Program Characterizes the Meiotic Transition of Male Germ Cells

To achieve a comprehensive characterization of the splicing changes occurring during transmeiotic differentiation of male germ cells, we performed high-throughput RNA sequencing (RNA-seq) analyses of poly(A)$^+$ RNA isolated from highly purified populations of meiotic spermatocytes (n = 2) and post-meiotic spermatids (n = 3) (Figure 1A). Gene expression analyses revealed a remarkable and global reprogramming of the transcriptome across meiosis, with 12,726 genes (corresponding to nearly 60% of the expressed genes; data not shown) differentially expressed between spermatocytes and spermatids (Figure 1B). As expected, transcripts for the spermatid-specific nucleoproteins (i.e., protamines and transition proteins) (Dadoune, 2003) and the sperm-specific calcium channels (i.e., CatSper proteins) (Singh and Rajender, 2015) were strongly upregulated in spermatids (Figure S1A). By contrast, expression of

the *Sycp2* and *Sycp3* genes, encoding synaptonemal proteins (Wang et al., 2005), and of *Mlh3* and *Spo11*, encoding homologous recombination proteins (Romanienko and Camerini-Otero, 2000; Santucci-Darmanin et al., 2002), were upregulated in spermatocytes (Figure S1A). These observations confirmed the purity of the germ cell populations and the reliability of the bioinformatics analysis.

By using the FAST-DB splicing patterns annotation tool, we also identified 4,090 AS events in 1,753 genes that are modulated across meiosis in male germ cells, with the majority (65.1%) being upregulated in spermatocytes (Figure 1C and Table S1). Classification of the events corresponding to annotated splice variants in the FAST-DB reference database highlighted selection of alternative first and last exons and IR as the most regulated splicing modalities (Figure 1D and Table S2). RT-PCR analysis of randomly selected events yielded a high validation rate in all splicing patterns (80%; 12/15 events tested) (Figures 1E and S1B). Moreover, comparison of our dataset with a previous RNA-seq analysis of spermatocyte and spermatid transcriptomes (GSE43717; Soumillon et al., 2013) revealed a highly significant overlap ($p = 0$; modified Fisher's test) in splicing-regulated genes (Figure S1C) and a very similar distribution of splicing patterns (Figure S1D). Although many splicing-regulated genes (44.8%) were also regulated at the expression level (Figure S1E), with almost equal frequency in all splicing patterns (Figure S1F), they were underrepresented when compared with the total of genes differentially expressed in the two cell types (60% of expressed genes). These results uncover an extended transcriptome reprogramming across meiosis and highlight a specific splicing program activated during this crucial phase of spermatogenesis.

Intron Retention Is a Specific Feature of the Meiotic Transcriptome

An unexpected finding of our analysis was the large extent of IR detected in male germ cells (Figure 1D). Indeed, unlike other splicing patterns, IR events were strikingly over-represented with respect to their expected frequency in the FAST-DB reference database (Figure 2A). To test whether this enrichment was due to underestimation of IR events in the FAST-DB, we analyzed RNA-seq data for other developing/differentiation systems using the same approach. Notably, in the comparison between the transcriptome of round spermatids and somatic Sertoli cells of the testis (GSE43717; Soumillon et al., 2013), IR accounted for 10% of the regulated splicing events, whereas this percentage was even lower (6%) when we compared newborn with adult cardiomyocytes (GSE49906; Giudice et al., 2014) (Figures S2A and S2B). By contrast, a similar percentage of IR events (22% compared with 29% in our condition) was regulated between spermatocyte and spermatid transcriptomes from an independent source (Soumillon et al., 2013) (Figures S1C and S2B). Thus, IR regulation is a specific feature of the trans-meiotic differentiation of male germ cells.

Further classification of all splicing events differentially regulated between spermatocytes and spermatids (thus including novel splice variants besides the annotated ones of Figure 1C) showed that IR accounts for 40.9% of the regulated splicing events (Figure S2C). Notably, 80% of IR events were upregulated in spermatocytes compared with spermatids (Figure 2B). This trend was statistically significant and specific, as all other splicing types were more equally distributed among up- and downregulated events (Figure 2B). Moreover, analysis of IR regulation from an independent RNA-seq analysis of mouse spermatocytes and spermatids (Soumillon et al., 2013) yielded highly significant overlap with our results (Figures S2D–S2F). These analyses strongly suggest that IR represents a prominent modality of splicing regulation in meiotic spermatocytes. Time-course analysis of representative IR events in whole testis RNAs confirmed that introns are spliced more efficiently in adult testis (60 days post partum [dpp]), when the majority of germ cells are at post-meiotic stages, than in juvenile testis (12–20 dpp) (Figures S3A and S3B), when the organ is enriched in meiotic cells (Griswold, 2016).

To validate these observations, we selected a subset of IR events predicted by the RNA-seq analysis. In all 20 cases tested, real-time PCR analysis using primers spanning exon-intron regions and exon-exon junctions (spliced introns) confirmed much higher expression levels of IRTs in spermatocytes compared with both early-stage (round) and late-stage (elongated) spermatids (Figures 2C and S3C–S3E). IR events were specific, as neighboring introns not detected in the RNA-seq analysis were not significantly retained in spermatocytes (Figure 2C). Likewise, five genes that resulted properly spliced by RNA-seq analysis did not display any significant accumulation of introns (Figure S3F). These results confirmed that IR is a prominent pattern in mouse spermatocytes, which affects a large proportion of their splicing signature.

Meiotic Intron-Retaining mRNAs Are Stable Nuclear Transcripts

Generation of IRTs in mammalian cells has been mainly described as a device utilized to downregulate expression of genes that are no longer required during stress or development (Wong et al., 2016). In these transcripts, IR often introduces premature termination codons (PTCs), thus targeting them to degradation by the non-sense-mediated decay (NMD) pathway or by the nuclear RNA quality-control machinery (Yap et al., 2012; Wong et al., 2013; Shalgi et al., 2014; Edwards et al., 2016; Pimentel et al., 2016; Ni et al., 2016). However, we observed no enrichment for downregulated genes within those affected by IR compared with other splicing-regulated genes (Figure 3A). On the contrary, IRTs are slightly enriched for unaffected and upregulated genes (Figure 3A). Furthermore, among the 542 IR events introducing PTCs that we predicted from in silico analysis, we did not observe enrichment for downregulated genes (Figure S4). These observations suggest that IR does not target transcripts for degradation in meiosis.

To directly test whether IR affects the stability of meiotic transcripts, we analyzed their decay after transcription inhibition. Fragments of testicular tubules were cultured for 4 hr in the presence of 5-Ethynyl uridine (EU), a nucleoside analog of uracil, to label nascent transcripts (Jao and Salic, 2008). After EU removal, transcription was inhibited by treatment with flavopiridol (FPD) and EU-labeled RNAs were isolated. Interestingly, FPD treatment did not cause a detectable reduction in the expression levels of IRTs (Figure 3B). By contrast, expression of properly spliced genes, such as *Gosr2*, *B2m*, *Grpel1*, or *Hspa4*, was reduced after transcriptional inhibition, similarly to what was observed for the high-turnover *Jun* transcript (Figure 3B).

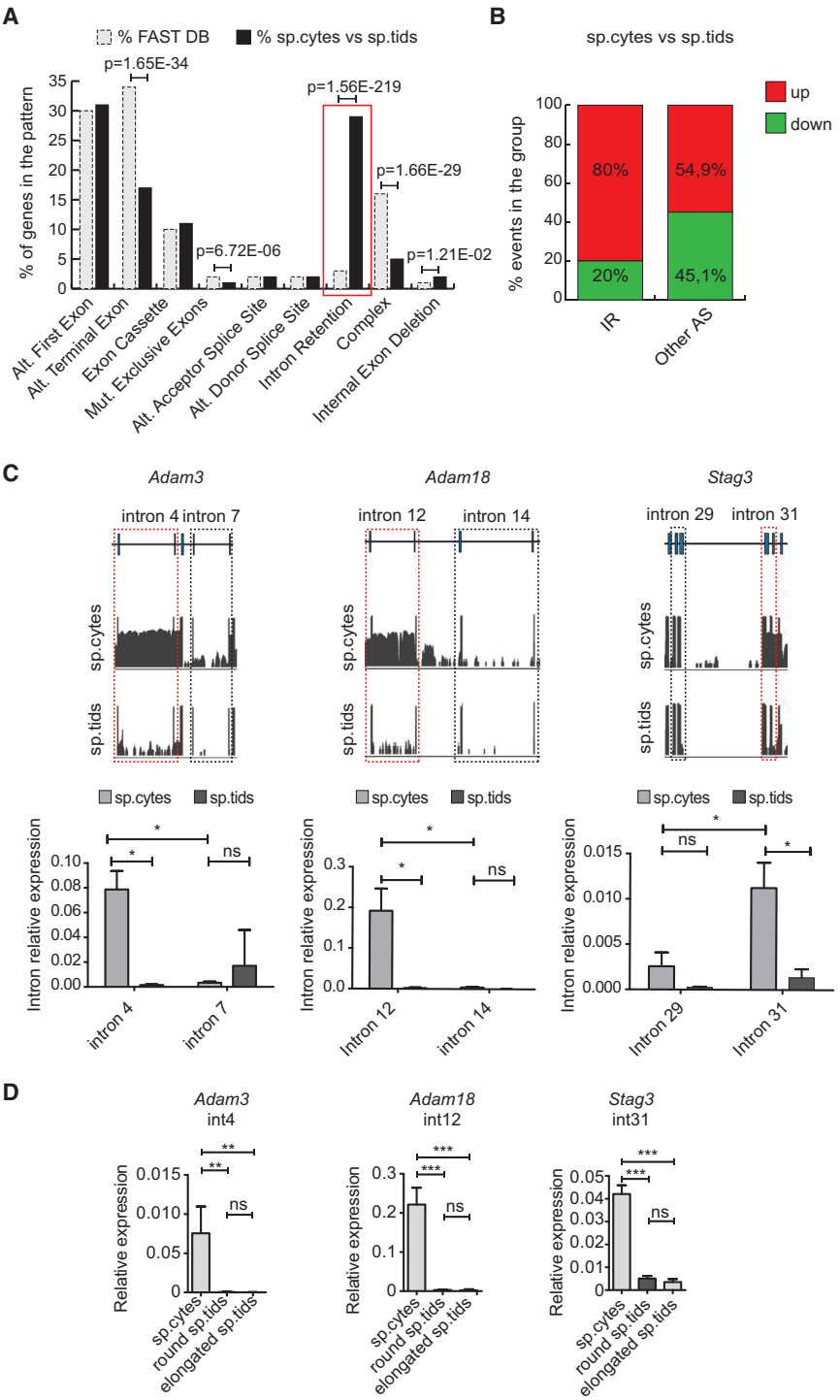

Figure 2. Intron Retention Is a Key Feature of the Male Meiotic Transcriptome

(A) Bar graph showing percentages of events annotated in FAST-DB (dashed, light gray columns) and of those differentially regulated between spermatocytes (sp.cytes) and spermatids (sp.tids) (black columns) within each AS pattern. p Values above the graph indicate a significant enrichment for regulated events within specific AS pattern in our dataset compared with the reference database (modified Fisher's test). Red box highlights the IR pattern.

(B) Bar graph representing percentages of up- and downregulated events among exonic and intronic splicing events. Enrichment in upregulated events in IR with respect to all other AS events was statistically significant ($p = 4.9 \times 10^{-61}$; χ^2 test).

(C) (Top) Visualization of the RNA-seq reads profile of the intron-retaining genes *Adam3*, *Adam18*, and *Stag3* in sp.cytes (upper graph) and sp.tids (lower graph). Sequence reads (vertical gray lines), exons (blue boxes), and introns (horizontal lines) are shown. (Bottom) Bar graphs showing results of qPCR analyses for the expression of the retained and non-retained introns (red and black dashed boxes, respectively) relative to their flanking exons in sp.cytes and sp.tids (mean ± SD, n = 3; $^*p \leq 0.05$, ns = not significant; one-way ANOVA).

(D) Bar graphs showing results of qPCR analyses for the expression of indicated introns relative to spliced product of their flanking exons in sp.cytes, and round and elongated sp.tids (mean ± SD, n = 4; $^{**}p \leq 0.01$, $^{***}p \leq 0.001$; ns, not significant; one-way ANOVA).

See also Figures S2 and S3.

Moreover, by comparing transcript levels in FPD versus vehicle-treated tubules, we observed a significantly higher stability for IRTs with respect to properly spliced transcripts (Figure 3C).

To further investigate the regulation of IR-containing transcripts, we checked their localization. Cellular fractionation followed by conventional PCR analysis demonstrated that IRTs (i.e., *Adam3*, *Izumo4*, and *Hook2* transcripts) were specifically localized in the nucleus of meiotic spermatocytes, whereas no signal for IRTs was detected in the nuclear fraction of spermatids (Figure 3D). These observations further confirmed the meiosis-specific nature of the IR phenomenon in male germ cells and suggest that nuclear localization of these transcripts may prevent their degradation. Thus, unlike what was observed in other differentiation processes, IR during spermatogenesis is not functional in dampening the regulated transcripts.

Transcriptional Overload Negatively Selects Splicing of Weak Introns in Meiosis

To gain insight into the nature of the IRTs enriched in meiosis, we explored whether retained introns displayed specific structural features that may distinguish them from properly spliced introns. Bioinformatics analysis documented that retained introns are preferentially localized toward the 3′ end of genes (Figure 4A). Similarly to what was previously reported for other introns affected by developmentally or physiologically regulated retention (Braunschweig et al., 2014; Boutz et al., 2015), meiotically retained introns are significantly shorter in length and display a higher GC content (Figures 4B and 4C). Furthermore, they are

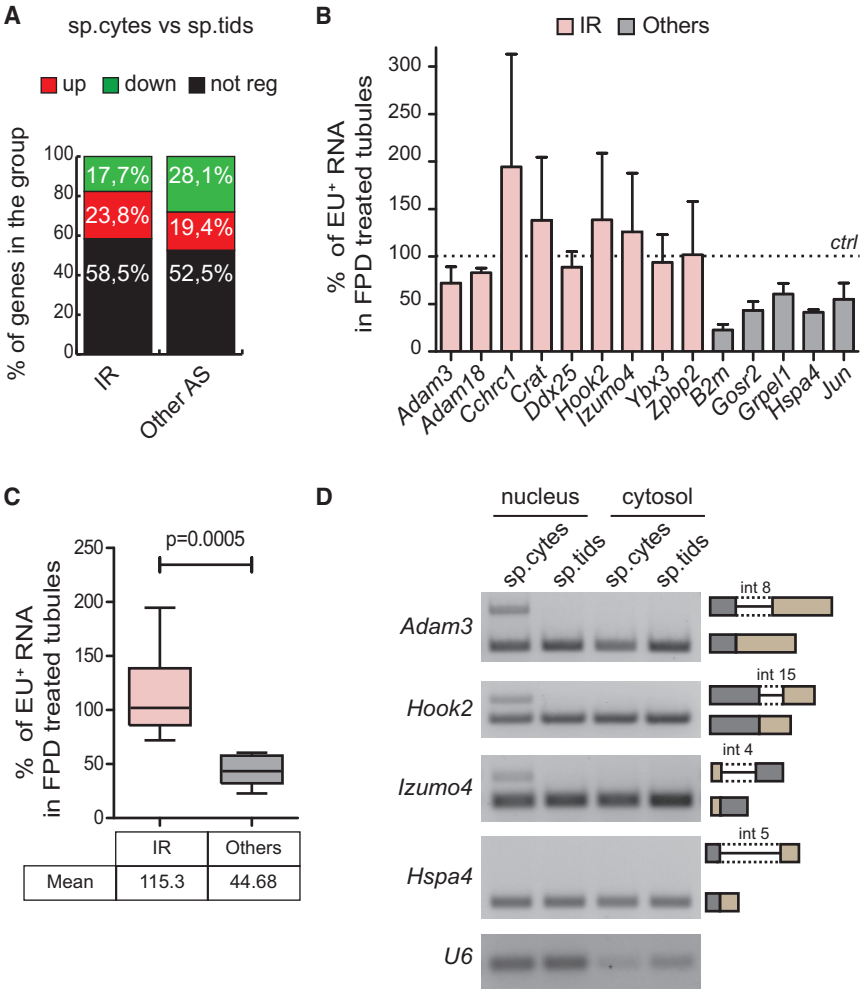

Figure 3. IRTs Are Highly Stable mRNAs Retained in the Nucleus of Meiotic Cells

(A) Bar graph showing percentages of expression-regulated genes within the groups of intron-retention and other splicing-regulated genes. A significant association was found between the gene regulation and the type of event ($p = 0.0156$; χ^2 test).

(B) Bar graph showing qPCR analysis using primers spanning exon-intron regions for EU-labeled RNA transcripts of indicated genes isolated from total RNA of seminiferous tubules of 20-dpp (days post-partum) mice treated or not for 1 hr with 1 μM FPD. Results are expressed as percentage of the EU-labeled RNA pulled down relative to control condition, arbitrarily set to 100% (dashed line in the graph, mean ± SD, n = 3).

(C) Box plot showing the distribution of the mean percentages of EU-labeled RNA transcripts pulled down as described in (B) in the IR-regulated genes and other expressed genes. Whiskers indicate 1.5 interquartile range. p Value indicates a significant difference between means of the two groups (Welch's t test).

(D) PCR analysis of the subcellular localization of the IRTs of *Adam3*, *Hook2*, and *Izumo4* genes. The properly spliced genes *Hspa4* and *U6* were evaluated as control.

See also Figure S4.

flanked by weaker 5′ and 3′ splice sites when compared with all other introns (Figure 4D). These results suggest that meiotically retained introns represent a distinct class characterized by specific features, which might contribute to the mechanism(s) underlying their retention. Intriguingly, by evaluating the mean FPKM (fragments per kilobase of transcript per million mapped reads) value as estimate of the gene expression levels (Trapnell et al., 2010), we observed significantly higher expression in the group of IR genes compared with all the other transcribed genes (Figure 4E). Moreover, comparison of our dataset with chromatin immunoprecipitation sequencing (ChIP-seq) analyses of histone marks in spermatocytes available from the GEO database (GSE49624; Hammoud et al., 2014) highlighted a significant enrichment of epigenetic marks of active transcription (i.e., acetylated H3K27, trimethylated H3K4) in the 5′ region of IR genes with respect to all other genes, whereas repressive marks (i.e., trimethylated H3K27) were not affected (Figure 4F). These results suggest that the high transcriptional level of IR genes combined with the specific features of their sequence negatively selects retained introns from recognition and excision by the spliceosome in meiosis.

Next, we asked why meiotically retained introns were properly spliced in spermatids. Transcription is discontinuous during spermatogenesis, with three active bursts in mitotic spermatogonia, meiotic spermatocytes, and haploid early spermatids being followed by transcriptionally inactive phases (Paronetto and Sette, 2010). Measurement of total RNA per cell showed much higher levels in spermatocytes than in later stages of male germ cell differentiation (Figure 5A). Fast transcription elongation rates correlate with increased phosphorylation of RNAPII in serine 2 (Ser-2) (Phatnani and Greenleaf, 2006). Immunofluorescence analysis of seminiferous tubules and western blot analysis of isolated germ cells revealed strong Ser-2 phosphorylation of RNAPII in spermatocytes and much lower signal in round spermatids (Figures 5B and 5C), while no staining was detected in elongated spermatids (Figure 5B). Moreover, a short pulse of EU labeling showed higher levels of nascent transcripts in meiotic spermatocytes than in post-meiotic spermatids, which positively correlated with Ser-2 RNAPII staining (Figure S5). These observations indicate that spermatocytes display higher transcriptional activity than spermatids.

We hypothesized that the high levels of pre-mRNA synthesis in spermatocytes could impose competition for spliceosome recruitment, thus causing retention of introns with weak features (Figure 4D) in highly expressed transcripts such as IRTs (Figure 4E). To test whether release of this transcriptional burden allows splicing of retained introns, we treated fragments of testicular tubules with 5,6-dichloro-1-β-D-ribofuranosylbenzimidazole (DRB) to reduce Ser-2 phosphorylation (Figure 5D), thus decreasing the RNAPII elongation rate (Ip et al., 2011). Strikingly, DRB treatment was sufficient to enhance splicing of retained

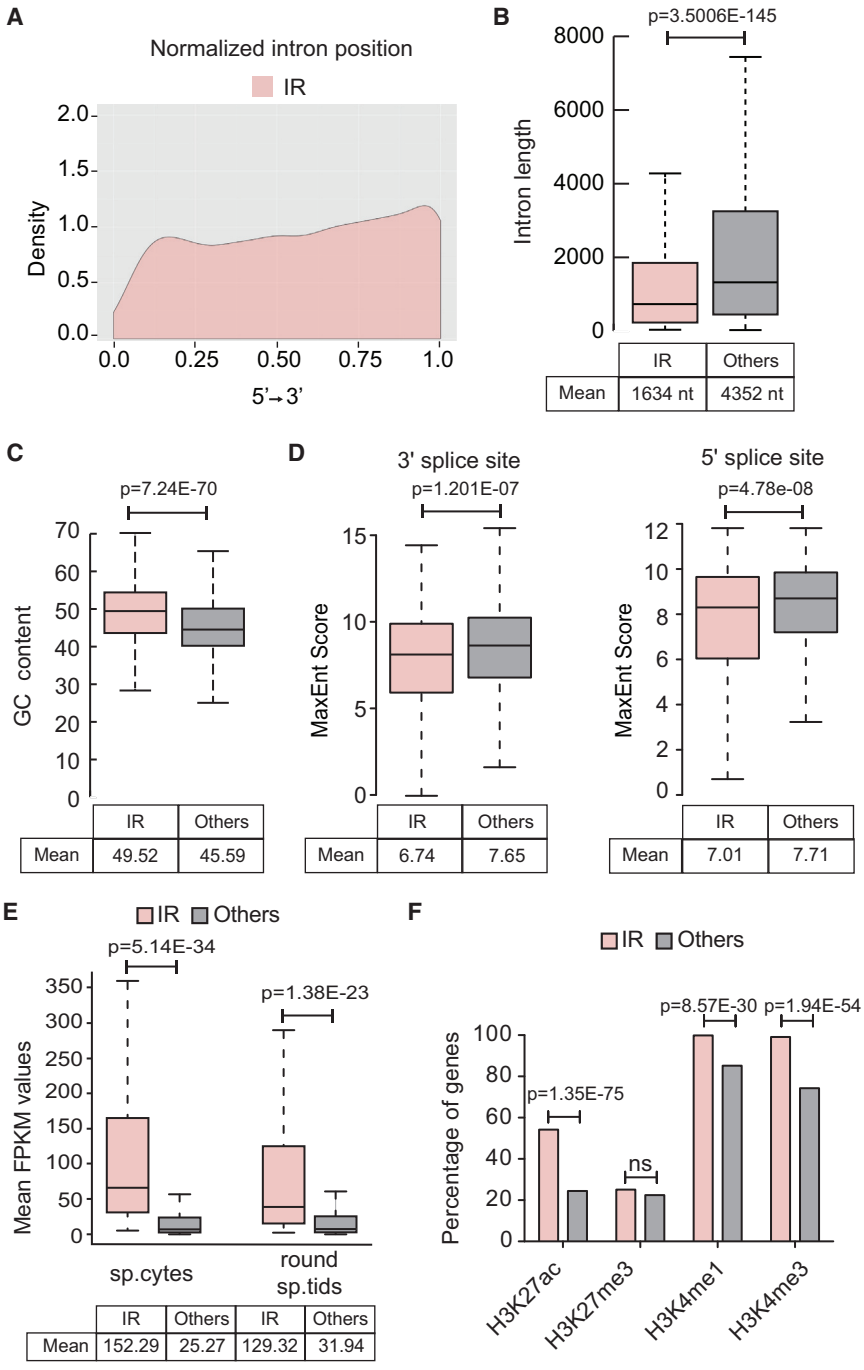

Figure 4. Specific *cis*-Acting Elements and Elevated Transcription Rate Feature Meiotic IRTs

(A) Graphic representation of retained introns location within gene body.

(B–D) Box plots representing comparison between retained introns and other introns for their length (B), GC content (C), and splice-site strength (D). Whiskers indicate 1.5 interquartile range. p Values indicate a significant difference between means of the two populations (Welch's t test).

(E) Box plots showing distribution of FPKM values for IR and other expressed genes in spermatocytes (sp.cytes) and spermatids (sp.tids). p Values indicate a significant difference between means of the two groups in the two cell types (Welch's t test).

(F) Bar graph showing percentages of intron-retaining and other expressed genes enriched for indicated histone marks in sp.cytes. p Values indicate a significant difference in the enrichment for different histone marks between the two groups (χ^2 test).

introns in IRTs (Figures 5D and 5E). These results show that reducing the transcription rate of mouse spermatocytes is sufficient to rescue recognition and splicing of retained introns by the spliceosome.

Meiotic Intron-Retaining Transcripts Are Preserved until Late Phases of Spermatogenesis and Encode for Key Spermatogenic Proteins

It was previously reported that a large amount of poly(A)$^+$ mRNAs is accumulated in the nucleus of spermatocytes, suggesting nuclear RNA storage at this stage of germ cell differentiation (Morales and Hecht, 1994). To examine whether mRNAs are actually stably stored in the nucleus of meiotic cells, we performed in vivo EU labeling of nascent RNAs and followed their fate upon germ cell differentiation (Figure 6A). Immunofluorescence analysis of testis 5 hr after EU injection indicated meiotic germ cells as the preferential site of accumulation of nascent RNAs in testis (Figure 6B). Importantly, these transcripts were stable for days in the nuclei of differentiating germ cells, as they were still detected in more luminal late meiotic (Figures 6C and 6D) and early post-meiotic germ cells (Figure S6A) even 9 days after EU injection. Stability of nuclear transcripts was a specific feature of germ cells, because it was not detected in the nuclei of the somatic Sertoli cells within the seminiferous tubules nor in the peritubular and interstitial cells of testis (Figure S6B). Furthermore, while EU-positive cells could be readily detected in kidney 5 hr after injection, no staining was present after 24 hr (Figure S6C).

Next, we asked whether IR promoted the accumulation of stable transcripts in spermatocyte nuclei. To this end, EU-labeled mRNAs were isolated by pull-down and analyzed by qPCR. We found that IRTs were stable in germ cells for up to 9 days after their synthesis, whereas the turnover of properly spliced mRNAs was much faster (Figure 6E). Indeed, ~50% of EU-labeled IRTs were still present after 24 hr and ~3%–10% of them were stored up to 9 days after labeling. By contrast, less than 10% of properly spliced mRNAs were detected 24 hr after labeling whereas they were undetectable after 9 days (Figure 6E). The higher stability in vivo of IRTs with respect to properly spliced transcripts was

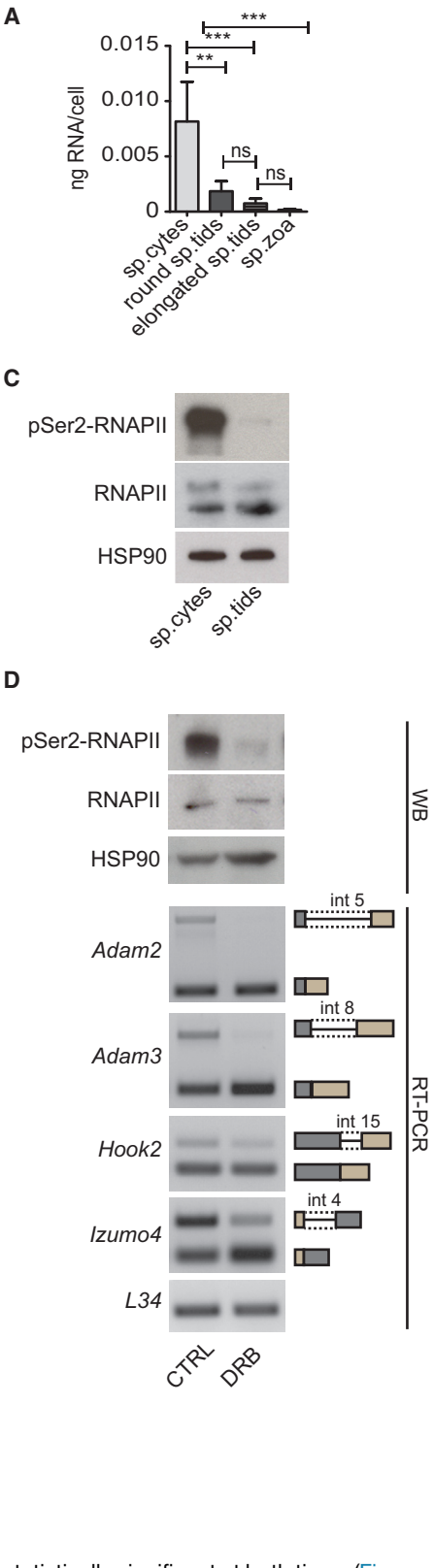

Figure 5. The Elevated Transcriptional Activity of Meiotic Spermatocytes Modulates IR Events

(A) Histogram showing the total RNA per cell synthesized by spermatocytes (sp.cytes), round spermatids (sp.tids), elongated sp.tids, and spermatozoa (sp.zoa) (mean ± SD, n = 4, $^{**}p \leq 0.01$, $^{***}p \leq 0.001$; ns, not significant; one-way ANOVA test).

(B) Representative images of immunofluorescence analysis of seminiferous tubule cross-sections from adult mice using anti-pSer2-RNAPII (H5) antibody. Hoechst staining was used to identify nuclear morphology. Insets show magnified images of meiotic spermatocytes (arrowhead), postmeiotic round spermatids (arrow), and elongated spermatids (square-headed arrow). Scale bar, 25 μm.

(C) Representative western blot analysis for RNAPII and its Ser2-CTD phosphorylated form (pSer2-RNAPII) in nuclear-enriched extracts of sp.cytes and round sp.tids. HSP90 protein level was evaluated as loading control.

(D) Upper panels show representative western blot analysis for total and pSer2-RNAPII in nuclear-enriched extracts obtained from seminiferous tubules treated or not for 24 hr with 10 μg/mL DRB. HSP90 was evaluated as loading control. Lower panels show representative images of agarose gel analysis for RT-PCR products of indicated IR events under the same experimental conditions.

(E) Bar graphs showing results of qPCR analyses for indicated retained introns relative to their flanking exons in seminiferous tubules treated for 24 hr with 10 μg/mL DRB compared with the control condition, arbitrarily set to 1 (mean ± SD, n = 4; $^{*}p \leq 0.05$, $^{**}p \leq 0.01$, $^{***}p \leq 0.001$; one-way ANOVA).

See also Figure S5.

statistically significant at both times (Figures 6F and 6G) and not influenced by levels of initial labeling, as IRTs did not show higher labeling efficiency (percentage of total RNA) 5 hr after EU injection (Figure S6D). These observations indicate that IR promotes nuclear accumulation and storage of a specific subset of transcripts in meiosis.

Post-transcriptional regulation of gene expression plays a key role during spermatogenesis (Paronetto and Sette, 2010), and some meiotic mRNAs are preserved and translated at later stages (Monesi, 1964; Geremia et al., 1977; Iguchi et al., 2006). To investigate whether IR genes displayed distinct functional properties with respect to all other AS-regulated genes, we performed gene ontology (GO) analysis. Notably, IR genes were specifically enriched in functional categories with strong relevance for spermatogenesis, and in particular for the late phase of this process when de novo mRNA synthesis is abolished (Monesi, 1964; Geremia et al., 1977) (Figure 7A). To test whether usage of IRTs is delayed during germ cell differentiation, we performed polysome profiling of testicular extracts at different times from EU injection. As previously suggested (Messina et al., 2010),

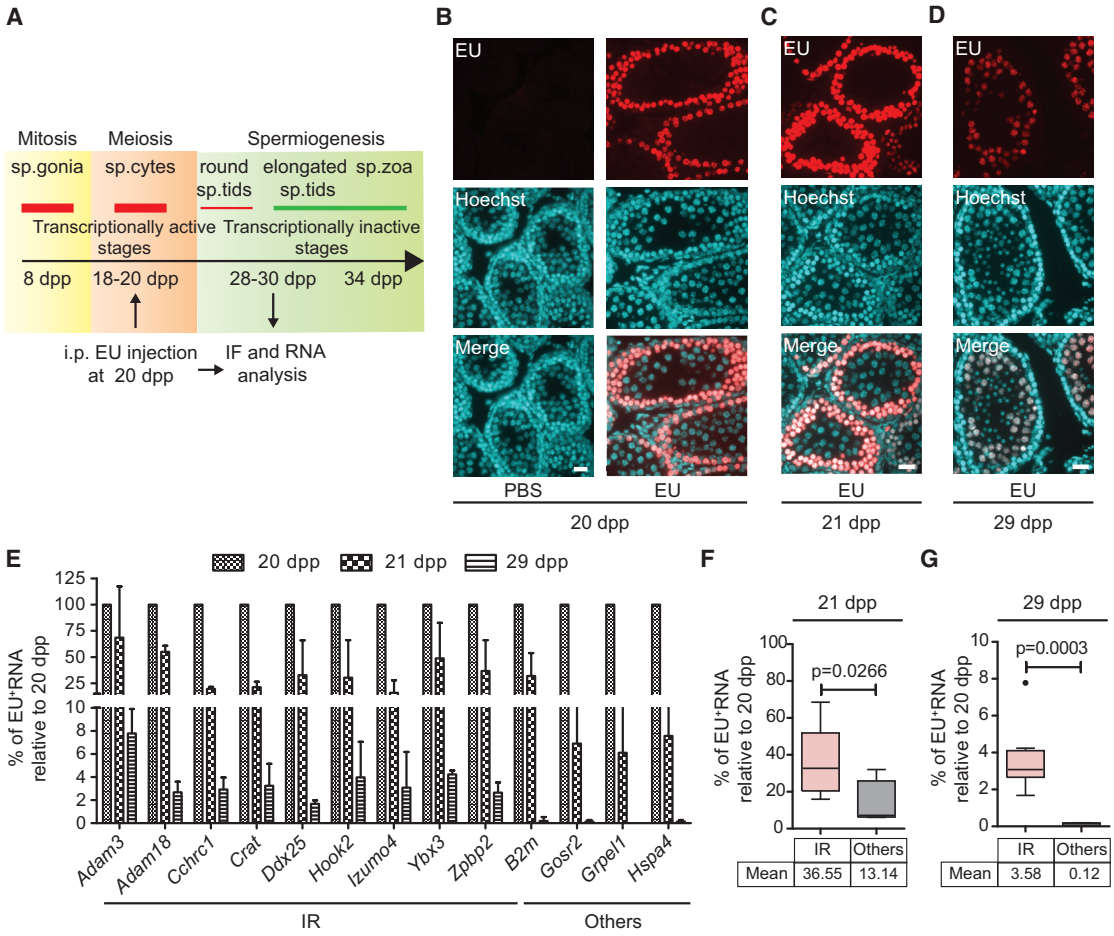

Figure 6. IRTs Are Stable during Spermatogenesis

(A) Schematic representation of the timeline of the key phases of murine spermatogenesis and their transcriptional activity. Time points of the in vivo RNA labeling experiments with EU are depicted below.

(B–D) EU staining with Alexa 594-azide of testicular paraffin-embedded cross-sections from EU-injected and PBS-injected (as control) mice harvested at 20 dpp (B), 21 dpp (C), and 29 dpp (D). Hoechst nuclear staining was performed to discriminate the different cellular types within the seminiferous tubules. Scale bar, 25 μm.

(E) Bar graph showing qPCR analysis for EU-labeled RNAs pulled down at indicated time points. Results are expressed as percentage of the EU-labeled RNA captured 5 hr after injection at 20 dpp, arbitrarily set to 100% (mean ± SD, n = 3).

(F and G) Box plot showing the distribution of the mean percentages of EU-labeled RNAs pulled down as described in (E) in the IR-regulated genes and other expressed genes. Whiskers indicate 1.5 interquartile range. p Values indicate a significant difference between means of the two groups (Welch's t test).

See also Figure S6.

translation efficiency was very low in testis (Figures 7B, S7A, and S7B), with transcripts being enriched in the translationally inactive "non-polysome" fractions (Figure S7C). However, we found that EU-labeled transcripts encoded by IR-regulated genes displayed a time-dependent shift to translationally active polysomes at times (9 days) (Figure 7C) when properly spliced transcripts have already disappeared (Figure 6E). This clear relative increase in transcript recruitment to the polysomes, however, may not result in more protein, as the total amount of transcripts decreases between day 21 and day 29 (Figure 6E). To test the possibility that proteins encoded by IR-regulated genes accumulate in late germ cells, we analyzed the expression of ADAM3 as a representative example. In line with the polysomal recruitment at later stages, ADAM3 protein levels steadily increased from spermatocytes to elongated spermatids (Figure 7D). These results suggest that IR is a mechanism designed to accumulate and preserve transcripts with strong relevance for gamete differentiation, thus prolonging their use until later stages of spermatogenesis.

DISCUSSION

Testis displays the highest transcriptome complexity among mammalian tissues, and most of this complexity is due to germ cells undergoing differentiation (Soumillon et al., 2013). Although AS is known to amplify transcriptome diversity (Fu and Ares, 2014) and testis is characterized by a high content of tissue-specific splice variants (Kan et al., 2005; Schmid et al., 2013), scant

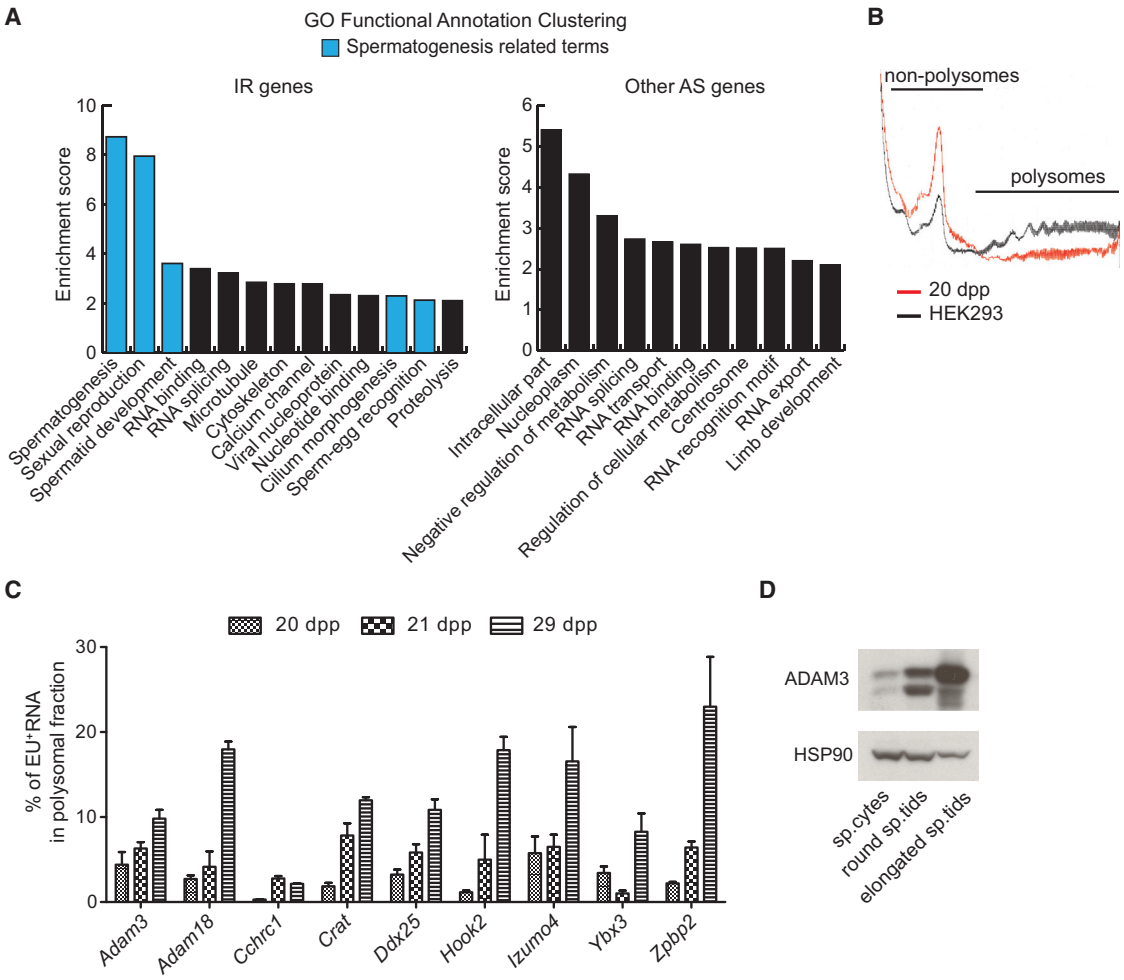

Figure 7. Meiotic IRTs Are Enriched in GO Terms Relative to Spermatogenesis and Are Actively Translated Several Days after Their Synthesis

(A) Bar graphs showing the enrichment score of the GO functional clusters enriched in the groups of IR-regulated and other AS-regulated genes ($p \leq 0.05$, high stringency).

(B) Absorbance profile (OD = 260 nm) of sucrose gradient sedimentation of extracts from mitotic HEK293 cells (black line) and testes of 20-dpp mice (red line).

(C) Bar graphs showing results of qPCR analysis for EU-labeled RNAs of indicated genes within the polysomal fraction derived from sucrose gradient fractionation of whole testes harvested at indicated time points after EU injection at 20 dpp. Results are expressed as percentage of the total EU-labeled RNA in all the fractions of the gradient (mean ± SD, n = 3).

(D) Representative images of western blot analysis for ADAM3 in total extracts of spermatocytes (sp.cytes), and round and elongated spermatids (sp.tids). HSP90 was evaluated as loading control.

See also Figure S7.

information is available on the global splicing changes occurring during germ cell differentiation. Here we uncovered a widespread IR program in meiosis, which stabilizes highly expressed transcripts with strong relevance for spermatogenesis. IRTs are retained in the nucleus of meiotic cells for days and can be recruited onto the polysomes for translation long after their synthesis. Thus our results indicate that, in addition to being a device to destabilize transcripts at specific developmental transitions (Yap et al., 2012; Wong et al., 2013; Shalgi et al., 2014; Edwards et al., 2016; Pimentel et al., 2016; Ni et al., 2016), IR can also favor accumulation, storage, and timely usage of specific transcripts during highly organized cell differentiation programs, such as spermatogenesis. A similar "positive" role for IR was also described in embryonic stem cells in response to stress (Boutz et al., 2015). However, the peculiarity of our finding is that IRTs can be maintained for days after synthesis and that IR regulation timely determines the usage of transcripts when transcription is repressed. This observation suggests that post-transcriptional splicing is particularly suited to temporally control gene expression in cells undergoing transcriptional silencing, such as germ cells at specific stages of their differentiation (Paronetto and Sette, 2010).

Meiotic spermatocytes and post-meiotic spermatids were selected for analyses because these cells undergo profound and unique morphogenetic changes, such as homologous recombination and spermiogenesis (Griswold, 2016), which likely require a global reprogramming of gene expression. Accordingly, we found that ~60% of the transcribed genome

is differentially regulated between these cell types, indicating a widespread reorganization of the transcriptome across meiosis. In addition to changes in transcript levels, our analyses also highlighted an extensive AS program regulated during transmeiotic differentiation of germ cells. We focused on IR because it was the most represented pattern, far beyond its expected frequency, and because intron-retaining genes were enriched in functional categories strongly relevant for spermatogenesis with respect to all other AS-regulated genes. Most IR events were detected in meiotic spermatocytes, whereas these introns were spliced in post-meiotic cells. These observations suggested that temporal regulation of IR plays an important role in male germ cell differentiation. One question arising from these results is why retained introns are less efficiently spliced in meiotic cells. Interestingly, bioinformatics analyses identified sequence features (i.e., weak splice sites, short length, high GC content) that were also found in retained introns in other cell types and tissues (Braunschweig et al., 2014). In addition, we found that IRTs are expressed at significantly higher level than all other transcripts in the germ cell transcriptome. In line with the observations that spermatocytes display higher transcriptional rates (Monesi, 1964; Geremia et al., 1977; Paronetto et al., 2011) and RNAPII phosphorylated levels (Ser2) than post-meiotic spermatids (this work), we hypothesized that meiotically retained introns could be outcompeted by stronger introns during co-transcriptional splicing. In support of this hypothesis, we found that relieving this "transcriptional burden" by reducing RNAPII activity rescued splicing of retained introns in meiotic cells, thus recapitulating the pattern observed in spermatids. Notably, a similar developmentally modulated competition for the spliceosome was also described in yeast (Munding et al., 2013). In that case, however, high transcription of ribosomal genes titrated the splicing machinery away from weak introns and favored their retention in vegetative cells. When ribosomal genes are turned off in meiosis, splicing efficiency is restored (Munding et al., 2013), indicating that pre-mRNAs compete for limiting factors during nuclear processing. Thus, modulation of IR by competition for the spliceosome could represent a conserved mechanism of regulation for genes involved in specialized developmental programs in eukaryotes.

One key feature of mammalian spermatogenesis is the discontinuous nature of transcription. In particular, de novo synthesis of mRNAs is ceased in post-meiotic cells due to exchange of histones with protamines and tight compaction of the chromatin (Paronetto and Sette, 2010; Hermo et al., 2010b). Thus, transcripts required for the late phases of differentiation must be synthesized prematurely and stored until needed. While much of this regulation was attributed to translational control in the cytoplasm (Paronetto and Sette, 2010; Kleene, 2013), it was also observed that a large fraction of poly(A)$^+$ transcripts accumulated in the nucleus of meiotic spermatocytes (Morales and Hecht, 1994). Here we found that IRTs are highly expressed polyadenylated transcripts exclusively localized in the meiotic nuclei, which may account for this earlier observation. Moreover, fate-mapping experiments demonstrated that IRTs are particularly stable transcripts, suggesting that they might be stored in the nuclei to be utilized at later stages. Indeed, although we cannot formally prove that the spliced mRNAs recruited for translation directly derive from IRT molecules, polysome profiling indicated that their translational efficiency increases with time, likely as a reflection of their slow and delayed splicing. Since functional categories related to mature gamete properties, such as spermatid development and sperm-egg recognition, are significantly enriched in IR-regulated genes, we suggest that IR allows their accumulation during the transcriptional burst of meiotic cells, whereas the slower transcriptional rate of post-meiotic cells favors spliceosome recruitment, splicing, and translation. As a proof of principle of this hypothesis, we show that accumulation of ADAM3 protein parallels the delay in pre-mRNA processing and polysome recruitment of its transcript. Thus, IR might represent a device to temporally uncouple transcription and translation of abundant mRNAs that are required for proper sperm function.

In conclusion, our study expands the role of IR in the regulation of gene expression in mammals. While it was previously appreciated that IR promotes elimination of unwanted transcripts at developmental or differentiation transitions, we now show that it can also play a positive effect by ensuring timely expression of selected genes during highly specialized developmental programs.

STAR★METHODS

Detailed methods are provided in the online version of this paper and include the following:

- KEY RESOURCES TABLE
- CONTACT FOR REAGENT AND RESOURCE SHARING
- EXPERIMENTAL MODEL AND SUBJECT DETAILS
  - Mouse Husbandry and Male Germ Cells Isolation
  - Seminiferous Tubules Culture
- METHOD DETAILS
  - RNA Extraction, Library Preparation and RNA-Seq Data Analysis
  - Extraction of RNA, RT-PCR and Real-Time PCR Analysis
  - Analysis of Cis-Acting Features of Retained Introns
  - PTC and NMD Prediction
  - Comparison with ChIP-Seq Data
  - Protein Extracts and Western Blot Analysis
  - Immunofluorescence Analysis of Nascent RNAs
  - Pull-Down Assay of Nascent RNAs
  - Immunofluorescence Analysis
- QUANTIFICATION AND STATISTICAL ANALYSIS
- DATA AND SOFTWARE AVAILABILITY

SUPPLEMENTAL INFORMATION

Supplemental Information includes seven figures and three tables and can be found with this article online at http://dx.doi.org/10.1016/j.devcel.2017.03.003.

AUTHOR CONTRIBUTIONS

Conceptualization, C.N and C.S.; Methodology, C.N., C.S., N.S., A.J.A., E.V., and R.G.; Software, Formal Analysis, and Data Curation, A.J. and P.D.I.G.; Investigation, C.N., S.D.P., N.S., and P.B.; Writing – Original Draft and Review & Editing, C.N. and C.S.; Visualization, C.N. and C.S.; Supervision, Project Administration, and Funding Acquisition, C.S.

ACKNOWLEDGMENTS

We thank Dr. Eleonora Cesari and Livia Pellegrini for technical assistance. This work was supported by grants from Telethon (GGP 12189; GGP 14095), Associazione Italiana Ricerca sul Cancro (AIRC; IG14581), and Ministry of Health "Ricerca Corrente" and "5x1000 Anno 2014" to Fondazione Santa Lucia.

Received: August 23, 2016
Revised: January 24, 2017
Accepted: March 3, 2017
Published: March 30, 2017

REFERENCES

Barbosa-Morais, N.L., Irimia, M., Pan, Q., Xiong, H.Y., Gueroussov, S., Lee, L.J., Slobodeniuc, V., Kutter, C., Watt, S., Colak, R., et al. (2012). The evolutionary landscape of alternative splicing in vertebrate species. Science *338*, 1587–1593.

Boutz, P.L., Bhutkar, A., and Sharp, P.A. (2015). Detained introns are a novel, widespread class of post-transcriptionally spliced introns. Genes Dev. *29*, 63–80.

Braunschweig, U., Barbosa-Morais, N.L., Pan, Q., Nachman, E.N., Alipanahi, B., Gonatopoulos-Pournatzis, T., Frey, B., Irimia, M., and Blencowe, B.J. (2014). Widespread intron retention in mammals functionally tunes transcriptomes. Genome Res. *24*, 1774–1786.

Chalmel, F., and Rolland, A.D. (2015). Linking transcriptomics and proteomics in spermatogenesis. Reproduction *150*, R149–R157.

Dadoune, J.P. (2003). Expression of mammalian spermatozoal nucleoproteins. Microsc. Res. Tech. *61*, 56–75.

Dobin, A., Davis, C.A., Schlesinger, F., Drenkow, J., Zaleski, C., Jha, S., Batut, P., Chaisson, M., and Gingeras, T.R. (2013). STAR: ultrafast universal RNA-seq aligner. Bioinformatics *29*, 15–21.

Edwards, C.R., Ritchie, W., Wong, J.J., Schmitz, U., Middleton, R., An, X., Mohandas, N., Rasko, J.E., and Blobel, G.A. (2016). A dynamic intron retention program in the mammalian megakaryocyte and erythrocyte lineages. Blood, pii:blood-2016-01-692764.

Fu, X.D., and Ares, M., Jr. (2014). Context-dependent control of alternative splicing by RNA-binding proteins. Nat. Rev. Genet. *15*, 689–701.

Furney, S.J., Pedersen, M., Gentien, D., Dumont, A.G., Rapinat, A., Desjardins, L., Turajlic, S., Piperno-Neumann, S., de la Grange, P., Roman-Roman, S., et al. (2013). SF3B1 mutations are associated with alternative splicing in uveal melanoma. Cancer Discov. *3*, 1122–1129.

Gandoura, S., Weiss, E., Rautou, P.E., Fasseu, M., Gustot, T., Lemoine, F., Hurtado-Nedelec, M., Hego, C., Vadrot, N., Elkrief, L., et al. (2013). Gene- and exon-expression profiling reveals an extensive LPS-induced response in immune cells in patients with cirrhosis. J. Hepatol. *58*, 936–948.

Geremia, R., Goldberg, R.B., and Bruce, W.R. (1976). Kinetics of histone and protamine synthesis during meiosis and spermiogenesis in the mouse. Andrologia *8*, 147–156.

Geremia, R., Boitani, C., Conti, M., and Monesi, V. (1977). RNA synthesis in spermatocytes and spermatids and preservation of meiotic RNA during spermiogenesis in the mouse. Cell Differ. *5*, 343–355.

Giudice, J., Xia, Z., Wang, E.T., Scavuzzo, M.A., Ward, A.J., Kalsotra, A., Wang, W., Wehrens, X.H., Burge, C.B., Li, W., et al. (2014). Alternative splicing regulates vesicular trafficking genes in cardiomyocytes during postnatal heart development. Nat. Commun. *5*, 3603.

Godmann, M., Auger, V., Ferraroni-Aguiar, V., Di Sauro, A., Sette, C., Behr, R., and Kimmins, S. (2007). Dynamic regulation of histone H3 methylation at lysine 4 in mammalian spermatogenesis. Biol. Reprod. *77*, 754–764.

Griswold, M.D. (2016). Spermatogenesis: the commitment to meiosis. Physiol. Rev. *96*, 1–17.

Hammoud, S.S., Low, D.H., Yi, C., Carrell, D.T., Guccione, E., and Cairns, B.R. (2014). Chromatin and transcription transitions of mammalian adult germline stem cells and spermatogenesis. Cell Stem Cell *15*, 239–253.

Hermo, L., Pelletier, R.M., Cyr, D.G., and Smith, C.E. (2010a). Surfing the wave, cycle, life history, and genes/proteins expressed by testicular germ cells. Part 1: background to spermatogenesis, spermatogonia, and spermatocytes. Microsc. Res. Tech. *73*, 241–278.

Hermo, L., Pelletier, R.M., Cyr, D.G., and Smith, C.E. (2010b). Surfing the wave, cycle, life history, and genes/proteins expressed by testicular germ cells. Part 2: changes in spermatid organelles associated with development of spermatozoa. Microsc. Res. Tech. *73*, 279–319.

Huang da, W., Sherman, B.T., and Lempicki, R.A. (2009). Systematic and integrative analysis of large gene lists using DAVID bioinformatics resources. Nat. Protoc. *4*, 44–57.

Iguchi, N., Tobias, J.W., and Hecht, N.B. (2006). Expression profiling reveals meiotic male germ cell mRNAs that are translationally up- and down-regulated. Proc. Natl. Acad. Sci. USA *103*, 7712–7717.

Ip, J.Y., Schmidt, D., Pan, Q., Ramani, A.K., Fraser, A.G., Odom, D.T., and Blencowe, B.J. (2011). Global impact of RNA polymerase II elongation inhibition on alternative splicing regulation. Genome Res. *21*, 390–401.

Jao, C.Y., and Salic, A. (2008). Exploring RNA transcription and turnover in vivo by using click chemistry. Proc. Natl. Acad. Sci. USA *105*, 15779–15784.

Kalsotra, A., and Cooper, T.A. (2011). Functional consequences of developmentally regulated alternative splicing. Nat. Rev. Genet. *12*, 715–729.

Kan, Z., Garrett-Engele, P.W., Johnson, J.M., and Castle, J.C. (2005). Evolutionarily conserved and diverged alternative splicing events show different expression and functional profiles. Nucleic Acids Res. *33*, 5659–5666.

Kleene, K.C. (2013). Connecting cis-elements and trans-factors with mechanisms of developmental regulation of mRNA translation in meiotic and haploid mammalian spermatogenic cells. Reproduction *146*, R1–R19.

Margolin, G., Khil, P.P., Kim, J., Bellani, M.A., and Camerini-Otero, R.D. (2014). Integrated transcriptome analysis of mouse spermatogenesis. BMC Genomics *15*, 39.

Messina, V., Di Sauro, A., Pedrotti, S., Adesso, L., Latina, A., Geremia, R., Rossi, P., and Sette, C. (2010). Differential contribution of the MTOR and MNK pathways to the regulation of mRNA translation in meiotic and postmeiotic mouse male germ cells. Biol. Reprod. *83*, 607–615.

Monesi, V. (1964). Ribonucleic acid synthesis during mitosis and meiosis in the mouse testis. J. Cell Biol. *22*, 521–532.

Morales, C.R., and Hecht, N.B. (1994). Poly(A)+ ribonucleic acids are enriched in spermatocyte nuclei but not in chromatoid bodies in the rat testis. Biol. Reprod. *50*, 309–319.

Muciaccia, B., Boitani, C., Berloco, B.P., Nudo, F., Spadetta, G., Stefanini, M., de Rooij, D.G., and Vicini, E. (2013). Novel stage classification of human spermatogenesis based on acrosome development. Biol. Reprod. *89*, 60.

Munding, E.M., Shiue, L., Katzman, S., Donohue, J.P., and Ares, M., Jr. (2013). Competition between pre-mRNAs for the splicing machinery drives global regulation of splicing. Mol. Cell. *51*, 338–348.

Nantel, F., and Sassone-Corsi, P. (1996). CREM: a transcriptional master switch during the spermatogenesis differentiation program. Front. Biosci. *1*, d266–d269.

Ni, T., Yang, W., Han, M., Zhang, Y., Shen, T., Nie, H., Zhou, Z., Dai, Y., Yang, Y., Liu, P., et al. (2016). Global intron retention mediated gene regulation during CD4+ T cell activation. Nucleic Acids Res. *44*, 6817–6829.

Noli, L., Capalbo, A., Ogilvie, C., Khalaf, Y., and Ilic, D. (2015). Discordant growth of monozygotic twins starts at the blastocyst stage: a case study. Stem Cell Rep. *5*, 946–953.

Paronetto, M.P., and Sette, C. (2010). Role of RNA-binding proteins in mammalian spermatogenesis. Int. J. Androl. *33*, 2–12.

Paronetto, M.P., Zalfa, F., Botti, F., Geremia, R., Bagni, C., and Sette, C. (2006). The nuclear RNA-binding protein Sam68 translocates to the cytoplasm and associates with the polysomes in mouse spermatocytes. Mol. Biol. Cell. *17*, 14–24.

Paronetto, M.P., Messina, V., Bianchi, E., Barchi, M., Vogel, G., Moretti, C., Palombi, F., Stefanini, M., Geremia, R., Richard, S., et al. (2009). Sam68 regulates translation of target mRNAs in male germ cells, necessary for mouse spermatogenesis. J. Cell Biol. *185*, 235–249.

Paronetto, M.P., Messina, V., Barchi, M., Geremia, R., Richard, S., and Sette, C. (2011). Sam68 marks the transcriptionally active stages of spermatogenesis and modulates alternative splicing in male germ cells. Nucleic Acids Res. *39*, 4961–4974.

Phatnani, H.P., and Greenleaf, A.L. (2006). Phosphorylation and functions of the RNA polymerase II CTD. Genes Dev. *20*, 2922–2936.

Pimentel, H., Parra, M., Gee, S.L., Mohandas, N., Pachter, L., and Conboy, J.G. (2016). A dynamic intron retention program enriched in RNA processing genes regulates gene expression during terminal erythropoiesis. Nucleic Acids Res. *44*, 838–851.

Rio, D.C., Ares, M., Jr., Hannon, G.J., and Nilsen, T.W. (2010). Preparation of cytoplasmic and nuclear RNA from tissue culture cells. Cold Spring Harb. Protoc. *2010*, http://dx.doi.org/10.1101/pdb.prot5441, pdb.prot5441.

Romanienko, P.J., and Camerini-Otero, R.D. (2000). The mouse Spo11 gene is required for meiotic chromosome synapsis. Mol. Cell. *6*, 975–987.

Santucci-Darmanin, S., Neyton, S., Lespinasse, F., Saunières, A., Gaudray, P., and Paquis-Flucklinger, V. (2002). The DNA mismatch-repair MLH3 protein interacts with MSH4 in meiotic cells, supporting a role for this MutL homolog in mammalian meiotic recombination. Hum. Mol. Genet. *11*, 1697–1706.

Schmid, R., Grellscheid, S.N., Ehrmann, I., Dalgliesh, C., Danilenko, M., Paronetto, M.P., Pedrotti, S., Grellscheid, D., Dixon, R.J., Sette, C., et al. (2013). The splicing landscape is globally reprogrammed during male meiosis. Nucleic Acids Res. *41*, 10170–10184.

Sette, C., Bevilacqua, A., Bianchini, A., Mangia, F., Geremia, R., and Rossi, P. (1997). Parthenogenetic activation of mouse eggs by microinjection of a truncated c-kit tyrosine kinase present in spermatozoa. Development *124*, 2267–2274.

Shalgi, R., Hurt, J.A., Lindquist, S., and Burge, C.B. (2014). Widespread inhibition of posttranscriptional splicing shapes the cellular transcriptome following heat shock. Cell Rep. *7*, 1362–1370.

Singh, A.P., and Rajender, S. (2015). CatSper channel, sperm function and male fertility. Reprod. Biomed. Online *30*, 28–38.

Soumillon, M., Necsulea, A., Weier, M., Brawand, D., Zhang, X., Gu, H., Barthès, P., Kokkinaki, M., Nef, S., Gnirke, A., et al. (2013). Cellular source and mechanisms of high transcriptome complexity in the mammalian testis. Cell Rep. *3*, 2179–2190.

Trapnell, C., Williams, B.A., Pertea, G., Mortazavi, A., Kwan, G., van Baren, M.J., Salzberg, S.L., Wold, B.J., and Pachter, L. (2010). Transcript assembly and quantification by RNA-Seq reveals unannotated transcripts and isoform switching during cell differentiation. Nat. Biotechnol. *28*, 511–515.

Traunmüller, L., Gomez, A.M., Nguyen, T.M., and Scheiffele, P. (2016). Control of neuronal synapse specification by a highly dedicated alternative splicing program. Science *352*, 982–986.

Wang, P.J., Page, D.C., and McCarrey, J.R. (2005). Differential expression of sex-linked and autosomal germ-cell-specific genes during spermatogenesis in the mouse. Hum. Mol. Genet. *14*, 2911–2918.

Wang, E., Aslanzadeh, V., Papa, F., Zhu, H., de la Grange, P., and Cambi, F. (2012). Global profiling of alternative splicing events and gene expression regulated by hnRNPH/F. PLoS One *7*, e51266.

Wong, J.J., Ritchie, W., Ebner, O.A., Selbach, M., Wong, J.W., Huang, Y., Gao, D., Pinello, N., Gonzalez, M., Baidya, K., et al. (2013). Orchestrated intron retention regulates normal granulocyte differentiation. Cell *154*, 583–595.

Wong, J.J., Au, A.Y., Ritchie, W., and Rasko, J.E. (2016). Intron retention in mRNA: no longer nonsense: known and putative roles of intron retention in normal and disease biology. Bioessays *38*, 41–49.

Yang, X., Coulombe-Huntington, J., Kang, S., Sheynkman, G.M., Hao, T., Richardson, A., Sun, S., Yang, F., Shen, Y.A., Murray, R.R., et al. (2016). Widespread expansion of protein interaction capabilities by alternative splicing. Cell *164*, 805–817.

Yap, K., Lim, Z.Q., Khandelia, P., Friedman, B., and Makeyev, E.V. (2012). Coordinated regulation of neuronal mRNA steady-state levels through developmentally controlled intron retention. Genes Dev. *26*, 1209–1223.

Yeo, G., and Burge, C.B. (2004). Maximum entropy modeling of short sequence motifs with applications to RNA splicing signals. J. Comput. Biol. *11*, 377–394.

Zhou, H., Grubisic, I., Zheng, K., He, Y., Wang, P.J., Kaplan, T., and Tjian, R. (2013). Taf7l cooperates with Trf2 to regulate spermiogenesis. Proc. Natl. Acad. Sci. USA *110*, 16886–16891.

STAR★METHODS

KEY RESOURCES TABLE

REAGENT or RESOURCE	SOURCE	IDENTIFIER
Antibodies		
Rat anti-RNA polymerase II subunit B1 (phospho CTD Ser-2) clone 3E1	Millipore	Cat # 04-1571; RRID: AB_10627998
Rabbit polyclonal anti HSP 90α/β (H-114)	Santa Cruz	Cat # sc-7947; RRID: AB_2121235
Rabbit polyclonal anti-RNA polymerase II (N-20)	Santa Cruz	Cat # sc-899; RRID: AB_632359
Mouse monoclonal anti-ADAM3	Santa Cruz	Cat # sc-365288; RRID: AB_10846942
Mouse monoclonal [H5] to RNAPII H5	Abcam	Cat # ab24758; RRID: AB_2167352
Donkey polyclonal Cy3 conjugated Anti-Mouse IgM	Jackson Immunoresearch	Cat # 715-165-020; RRID: AB_2340811
Donkey whole antibody anti Rabbit IgG HRP-linked	GE Healthcare	Cat # NA934; RRID: AB_772206
Sheep HRP-linked F(ab')2 fragment anti mouse IgG	GE Healthcare	Cat # NA9310; RRID: AB_772193
Goat anti-rat IgG HRP-linked	Santa Cruz	Cat # sc-2032; RRID: AB_631755
Chemicals, Peptides, and Recombinant Proteins		
Collagenase from Clostridium histolyticum	Sigma Aldrich	Cat # C7657; CAS 9001-12-1
Dnase I from bovine pancreas	Sigma Aldrich	Cat # DN25; CAS 9003-98-9
Trypsin from bovine pancreas	Sigma Aldrich	Cat # T9201; CAS 9002-07-7
5,6-Dichlorobenzimidazole 1-β-D-ribofuranoside (DRB)	Sigma Aldrich	Cat # D1916; CAS 53-85-0
Flavopiridol hydrochloride hydrate (FPD)	Sigma Aldrich	Cat # F3055
EU	Life Technologies	Cat # E10345
Critical Commercial Assays		
miRNEasy minikit	Qiagen	Cat # 217004
TruSeq Stranded mRNA Library Prep Kit	Illumina	Cat # RS-122-2101
RNase-free DNase	Roche	Cat # 04 716 728 001
M-MLV reverse transcriptase	Promega	Cat # M170B
GoTaq	Promega	Cat # M3005
LightCycler 480 SYBR Green I Master	Roche	Cat # 04 887 352 001
RNasin Ribonuclease Inhibitor	Promega	Cat # N251B
Immunocruz Western Blotting Luminol Reagent	Santa Cruz	Cat # sc-2048
Click-IT RNA Imaging kit	Life Technologies	Cat # C10330
Click-IT Nascent RNA Capture kit	Life Technologies	Cat # C10365
SuperScript VILO cDNA Synthesis Kit	Life Technologies	Cat #11754-050
Deposited Data		
Raw and analyzed data	This paper	GSE95138
Raw data	Soumillon et al., 2013	GSE43717
Raw data	Giudice et al., 2014	GSE49906
Raw data	Hammoud et al., 2014	GSE49624
Mouse reference genome assembly mm10, GRCm38	Genome Reference Consortium	https://www.ncbi.nlm.nih.gov/grc/mouse
Mouse FAST DB v2013_2	GenoSplice technology	http://www.easana.com
Experimental Models: Organisms/Strains		
Mouse: C57BL/6	Animal facility of the University of Rome Tor Vergata	N/A
Oligonucleotides		
See Table S3 for primer sequences used for conventional and qPCR analysis	This paper	N/A
Software and Algorithms		
FastQC V0.11.2		http://www.bioinformatics.babraham.ac.uk/projects/fastqc/

(*Continued on next page*)

Continued

REAGENT or RESOURCE	SOURCE	IDENTIFIER
Picard-Tools V1.119		https://broadinstitute.github.io/picard/
Bedtools V2-2.20.1		http://bedtools.readthedocs.io/en/latest/
Rseqc V2.3.9		http://rseqc.sourceforge.net/
STARv2.4.0	Dobin et al., 2013	https://github.com/alexdobin/STAR
DAVID Functional annotation Tool (v6.8)	Huang da et al., 2009	https://david.ncifcrf.gov/
MaxEntScan tool	Yeo and Burge, 2004	http://genes.mit.edu/burgelab/maxent/Xmaxentscan_scoreseq.html
Python V2.7.6		https://www.python.org/
R V3.2.5		https://www.r-project.org
GraphPad Prism 5.0		http://www.graphpad.com/

CONTACT FOR REAGENT AND RESOURCE SHARING

Further information and requests for resources and reagents should be directed to and will be fulfilled by the Lead Contact, Claudio Sette (claudio.sette@uniroma2.it).

EXPERIMENTAL MODEL AND SUBJECT DETAILS

Mouse Husbandry and Male Germ Cells Isolation

C57BL/6 mice were maintained on a normal 12 hr light/dark cycle in the animal facility of the University of Rome Tor Vergata, according to the Guideline of the Italian Institute of Health (protocol n. 1088/2016-PR). Spermatocytes and spermatids were collected from 12-week-old mice by gravimetric decantation (Sta-put) (for RNA-seq experiments) or by centrifugal elutriation of testicular cellular suspension as described (Geremia et al., 1976; Paronetto et al., 2006). Testicular cellular suspensions were prepared from single animal for the Sta-put method or by pooling germ cells collected from 3 age-matched animals for the centrifugal elutriation. Briefly, testes were dissected from the albuginea membrane and mildly digested for 15 minutes in 0,25 mg/ml collagenase (Sigma Aldrich); 0,05 mg/ml DNase I (Sigma Aldrich) in EKRB (120,1 mM NaCl; 4,8mM KCl; 25,2 mM $NaHCO_3$; 1,2 mM KH_2PO_4; 1,2 mM $MgSO_4$; 1,3 mM $CaCl_2$; 11 mM glucose) at 32°C with constant shaking. Digestion was followed by two washes in EKRB and by further digestion in EKRB containing 1 mg/ml trypsin; 0,05 mg/ml DNase I (Sigma Aldrich) for 30 min at 30 °C. Digestion was stopped by adding 10% fetal calf serum and the released germ cells were collected after sedimentation of tissue debris. Germ cells were centrifuged for 10 min at 1500 rpm at 4 °C, the pellet resuspended in 20 ml of EKRB supplemented with 0,2% bovine serum albumin (BSA) and finally injected in the sample chamber of the Sta-put apparatus or of the elutriator. Homogeneity of cell populations was 80-85% (pachytene spermatocytes and elongated sp.tids), 95% (round spermatids) and was monitored by analysis by Hoechst-staining of nuclear-morphology. For spermatozoa collection, cauda of epididymis of adult mice were dissected, placed in a petri dish containing PBS and incised in order to allow the sperm to swim out for 5 min into the medium (Sette et al., 1997). Sperm suspension was then collected and further processed for subsequent analyses.

Seminiferous Tubules Culture

For seminiferous tubules culture, testes collected from 20 dpp or adult mice were dissected from the albuginea membrane and mildly digested for 15 minutes in 0,25 mg/ml collagenase (Sigma Aldrich) at 32°C with constant shaking. Following two washes in MEM (Sigma Aldrich), released seminiferous tubules were cultured in MEM, supplemented with 0,5% BSA, 1 mM sodium pyruvate, 2 mM sodium lactate, non-essential aminoacids (Gibco), at 32°C in a humified atmosphere containing 5% CO_2. For 5,6-Dichlorobenzimidazole 1-β-D-ribofuranoside (DRB) treatment experiments seminiferous tubules were treated with 10 μg/ml DRB (Sigma) or vehicle alone (DMSO) for 24 hr.

METHOD DETAILS

RNA Extraction, Library Preparation and RNA-Seq Data Analysis

For RNA-seq analysis, purified populations of meiotic spermatocytes (n=2) and post-meiotic round spermatids (n=3) were fractionated by Sta-put and total RNA was extracted and DNAse treated using the miRNEasy extraction kit (Qiagen) according to manufacturer's instruction. PolyA plus RNA-seq libraries were constructed according to Illumina's protocol and sequenced using a 100 bp single-end format on an Illumina HiSeq 2000. RNA-Seq data analysis was performed by GenoSplice technology (www.genopslice.com). Sequencing, data quality, reads repartition (e.g., for potential ribosomal contamination), and insert size estimation were performed using FastQC, Picard-Tools, Samtools and rseqc. Reads were mapped using STARv2.4.0 (Dobin et al., 2013). Gene expression regulation study was performed as already described (Noli et al., 2015) using Mouse FAST DB v2013_2 annotations. Only

genes expressed in at least sp.tids or sp.cytes were further analyzed. Genes were considered as expressed if their rpkm value was greater than 97,5% of the background rpkm value based on intergenic regions. Results were considered statistically significant for p-values $\leq$ 0.05 and fold-changes $\geq$ 1.5. Analysis at the splicing level was performed as already described (Traunmüller et al., 2016; Furney et al., 2013): first, by taking into account only exon reads and flanking exon-exon junction reads (''exon'' analysis) in order to potentially detect new alternative events that could be differentially regulated (i.e., without taking into account known alternative events); then, by taking into account known patterns (''pattern'' analysis) using the FAST DB splicing patterns annotation (i.e., for each gene, all possible splicing patterns were defined by comparing exon content of transcripts). All types of alternative events can be analyzed: Alternative first exons, alternative terminal exons, cassette exon, mutually exclusive exons, alternative 5' donor splice site, alternative 3' acceptor splice sites, intron retention, internal exon deletion and complex events corresponding to mix of several alternative event categories). ''exon'' and ''pattern'' analyses were based on the splicing-index calculation as previously described (Gandoura et al., 2013; Wang et al., 2012). Results were considered statistically significant for p-values $\leq$ 0.05 and fold-changes $\geq$1.5 for ''PATTERN'' and p-values $\leq$ 0.05 and fold-changes $\geq$ 2.0 for ''EXON''. Same procedures were carried out for analysis of downloaded published datasets (GSE43717, Soumillon et al., 2013; GSE49906, Giudice et al., 2014). Analysis for enriched GO functional clusters among IR and other AS regulated genes was performed using DAVID Functional annotation Tool (v6.8), using the expressed genes as background (Huang da et al., 2009). Ontologies were considered as enriched if fold enrichment $\geq$ 2.0 and p-value $\leq$ 0.05.

Extraction of RNA, RT-PCR and Real-Time PCR Analysis

Total RNA was extracted using Trizol reagent (Invitrogen) according to the manufacturer's instructions. Isolation of nuclear and cytoplasmic RNA was performed as described (Rio et al., 2010). Briefly, isolated germ cells were washed three times with ice-cold PBS by centrifuging at 1000 g for 5 min and then lysed with three volumes of cold buffer A (10 mM KCl; 1,5 mM $MgCl_2$; 20 mM TrisHCl; 1 mM DTT). Cellular lysates were incubated for 10 min on ice and then homogenized in a Dounce homogenizer by applying 15 strokes with a type B pestle. After addition of Triton X-100 to a final concentration of 0,1%, homogenates were centrifuged at 1500 g for 5 min at 4°C. Trizol was immediately added to the pellet nuclei, while supernatant corresponding to the cytosolic fraction was transferred in a new tube and three volumes of Trizol added. After digestion with RNase-free DNase (Roche), 250 ng - 1 μg of total RNA was retro-transcribed with oligo-dT primers, using M-MLV reverse transcriptase (Promega). cDNA was used as template for PCR (GoTaq, Promega) and reactions were analyzed on agarose or acrylamide gels. PCR analysis for validation of AS events was performed in triplicate. Quantitative real-time PCRs (RT-qPCR) were performed using LightCycler 480 SYBR Green I Master and the LightCycler 480 System (Roche), according to the manufacturer's instructions. Control reactions omitting M-MLV reverse transcriptase were also carried out. All primers used are listed in Table S3.

Analysis of Cis-Acting Features of Retained Introns

To visualize the preferential location of retained introns, the number of retained intron was normalized with the total number of introns in the corresponding gene. 3' and 5' splice-sites strengths of retained introns and other introns were scored using MaxEntScan tool (Yeo and Burge, 2004) and GC content for each intron sequence was obtained by weighing the GC count with its length.

PTC and NMD Prediction

The representative RefSeq transcript was selected for each of the 768 genes with intron retention event. In case no RefSeq transcript existed, the GenBank transcript with a higher number of exons was selected. Sequence of retained intron was then included in transcript sequence. Open Reading Frame (ORF) predictions were performed using ''find_orfs_with_trans'' from Python module Bio.SeqIO (Python V2.7.6) on these new transcript sequences. Only ORFs from frame +1, +2 and +3 and with defined stop were selected. If the coding sequence (CDS) start site was already known in the original transcript sequence, ORF with the same start was selected. If no CDS was already known, the longest ORF was selected. If distance between the predicted CDS stop and the last exon-exon junction was greater than 50 nucleotides, the corresponding transcript was predicted to be targeted by NMD.

Comparison with ChIP-Seq Data

For comparison with ChIP-seq dataset for histone modifications, bedgraph files from GSE49624 (Hammoud et al., 2014) were annotated after changing the mm9 coordinates into the corresponding mm10 coordinates. The proportion of genes from ''IR'' and ''Others'' groups that were present in the GSE49624 data and had histone marks (score>=10) were plotted using R. These proportions were compared using Chi2 test, or Fisher's test when Chi2 conditions were not met (i.e. when expected values of the number of sample observations were < 5).

Protein Extracts and Western Blot Analysis

Nuclear-enriched cellular extracts were prepared by resuspending isolated germ cells or seminiferous tubules in RSB100 buffer [10 mM Tris HCl pH 7.4; 100 mM NaCl; 2,5 mM $MgCl_2$; 0,5 % (v/v) Triton X-100; 15 mM β-glycerophosphate; 1 mM DTT; 0,5 mM $NaVO_3$; protease inhibitor cocktail (Sigma Aldrich); RNasin Ribonuclease inhibitor 40U/ml (Promega)]. After incubation on ice for 15 min, samples were sonicated, stratified on 30% sucrose cushion and centrifuged for 15 min at 7000 g at 4°C. For total cellular extracts, isolated germ cells were resuspended in RIPA buffer [50 mM Tris pH 7.4; 1% NP-40; 0,5% Na deoxycholate; 0,1% SDS; 150 mM NaCl; 1 mM EDTA; 1 mM DTT; 0,5 mM $NaVO_3$; protease inhibitor cocktail (Sigma Aldrich)], incubated on ice for

20 min, briefly sonicated, and centrifuged for 20 min at 12000 g at 4°C. Protein extracts were then analyzed by Western Blot using the following primary antibodies: rat anti-RNA polymerase II subunit B1 (phospho CTD Ser-2) clone 3E1 (Millipore; dilution 1:1000); rabbit anti-HSP90α/β (dilution 1:1000), anti- RNA polymerase II N-20 (dilution 1:1000) and mouse anti-ADAM3 (dilution 1:400) (Santa Cruz). Anti-rabbit, anti-mouse (GE Healthcare) and anti-rat (Santa Cruz) HRP-linked secondary antibodies were all used at 1:10000 dilution and ECL signal developed using Immunocruz Western Blotting Luminol Reagent (Santa Cruz).

Immunofluorescence Analysis of Nascent RNAs

Nascent RNAs were analyzed by immunofluorescence using the Click-IT RNA Imaging kit (Life Technologies). Seminiferous tubules from adult mice were grown for 2 hr 30 min in presence of 1 mM EU (Life Technologies) and then collected for analysis. For in vivo labeling, 20 dpp mice were intraperitoneally injected with 300 μg/gr EU (Life Technologies) or PBS, as control, and organs collected 5 hr, 24 hr (21 dpp), and 9 days (29 dpp) after injection. Samples were formalin-fixed, paraffin embedded and EU-staining performed according to manufacturer's instructions. Briefly, 5-μm paraffin sections were mounted on polylysine-coated slides, dewaxed and rehydrated as previously described (Muciaccia et al., 2013). After permeabilization in 0,5% Triton X-100 in PBS for 20 min, sections were stained with Alexa Fluor 594 or Alexa Fluor 488 azide and nuclei counterstained with Hoechst 33342. Images were taken using a DMI6000B inverted microscope (LEICA Geosystems) equipped with a Pan-Neofluar 40X /0.75 objective lens and elaborated with Photoshop (Adobe) for composing panels.

Pull-Down Assay of Nascent RNAs

Seminiferous tubules from 20 dpp mice were grown for 4 hr in presence of 1 mM EU (Life Technologies) or PBS as control. Following two washes in MEM, tubules were released for 1 hr in fresh medium added or not with 1 μM flavopiridol (FPD) (Sigma-Aldrich) and then harvested for analysis. For in vivo labeling, 20 dpp mice were intraperitoneally injected with 300 μg/gr EU (Life Technologies) or PBS as control and testes collected 5 hr, 24 hr (21 dpp), and 9 days (29 dpp) after injection. Samples were collected in Trizol or snap-frozen for polysome fractionation, performed as previously described (Paronetto et al., 2006, 2009). Briefly, testes were homogenized in lysis buffer [100 mM NaCl; 10 mM $MgCl_2$; 30 mM Tris-HCl pH 7.5; 1% Triton X-100; 1 mM DTT; 0,5 mM $NaVO_3$; protease inhibitor cocktail (Sigma Aldrich); RNasin Ribonuclease inhibitor 40U/ml (Promega)]. After 15 min of incubation on ice, lysates were centrifuged for 10 min at 12000 g at 4°C. Supernatants were loaded on a 15-50% (w/v) sucrose gradients and sedimented by ultracentrifugation for 2 hr at 37000 rpm in a Beckman SW41 rotor. UV-absorption (A260) profiles of polysome gradients were measured by UV detector (UVis-920; GE Healthcare) and each gradient was collected in 10 fractions of 1 ml each. Fractions 1–5 and 6-10 were pooled to generate polysomal and non-polysomal fractions respectively and RNA was isolated by phenol:chloroform extraction. Isolated total or fractionated EU-labeled RNA was biotinylated and captured using the Click-IT Nascent RNA Capture kit (Life Technologies) according to manufacturer's instructions. Captured nascent RNAs were retrotranscribed using the SuperScript VILO cDNA Synthesis Kit (Life Technologies) followed by RT-qPCR analysis performed as aforementioned.

Immunofluorescence Analysis

5-μm sections from paraffin embedded seminiferous tubules cross-sections were processed for immunofluorescence analysis as follows: sections were serially collected and mounted on polylysine-coated slides. Dewaxed and rehydrated sections were incubated in 10 mM sodium citrate, 0,05% Tween 20 pH 6.0 in a microwave oven for antigen retrieval at 750 W three times for 5 min. After permeabilization in 0,5% Triton X-100 in PBS for 15 min, sections were incubated with glycine 1 M in PBS for quenching autofluorescence and blocked 1 hr in a 0,1% Triton, 1% BSA, 5% donkey serum PBS solution. Sections were then incubated 2 hr at room temperature with primary antibody RNAPII H5 (1:200, Abcam) and then 1 hr with Cy3- conjugated anti-mouse IgM (1:500, Jackson Immunoresearch). Nuclei were counterstained with Hoechst 33342. Images were taken using a DMI6000B inverted microscope (LEICA Geosystems) equipped with a Pan-Neofluar 40X /0.75 objective lens and elaborated with Photoshop (Adobe) for composing panels.

QUANTIFICATION AND STATISTICAL ANALYSIS

Statistical analyses for differential gene expression, splicing changes, comparison of different datasets, analysis of cis-acting sequence features of introns, were performed in R according the statistical tests described in the figure legends. Statistical analyses for qPCR analysis were performed in GraphPad Prism according to the statistical tests described in the figure legends. Number of different cellular preparations or of animals independently analyzed is indicated by the "n" in each figure legend. In all figures, if p-value is not stated: *, p-value $\leq$ 0.05; **, p-value $\leq$ 0.01; ***, p-value $\leq$ 0.001.

DATA AND SOFTWARE AVAILABILITY

The RNA-seq data have been deposited in the GEO database under ID GEO: GSE95138.

Developmental Cell, Volume *41*

Supplemental Information

An Orchestrated Intron Retention Program in Meiosis Controls Timely Usage of Transcripts during Germ Cell Differentiation

Chiara Naro, Ariane Jolly, Sara Di Persio, Pamela Bielli, Niclas Setterblad, Antonio J. Alberdi, Elena Vicini, Raffaele Geremia, Pierre De la Grange, and Claudio Sette

Inventory of Supplemental Information

Supplemental Figures

Supplemental Tables

Supplemental Figures

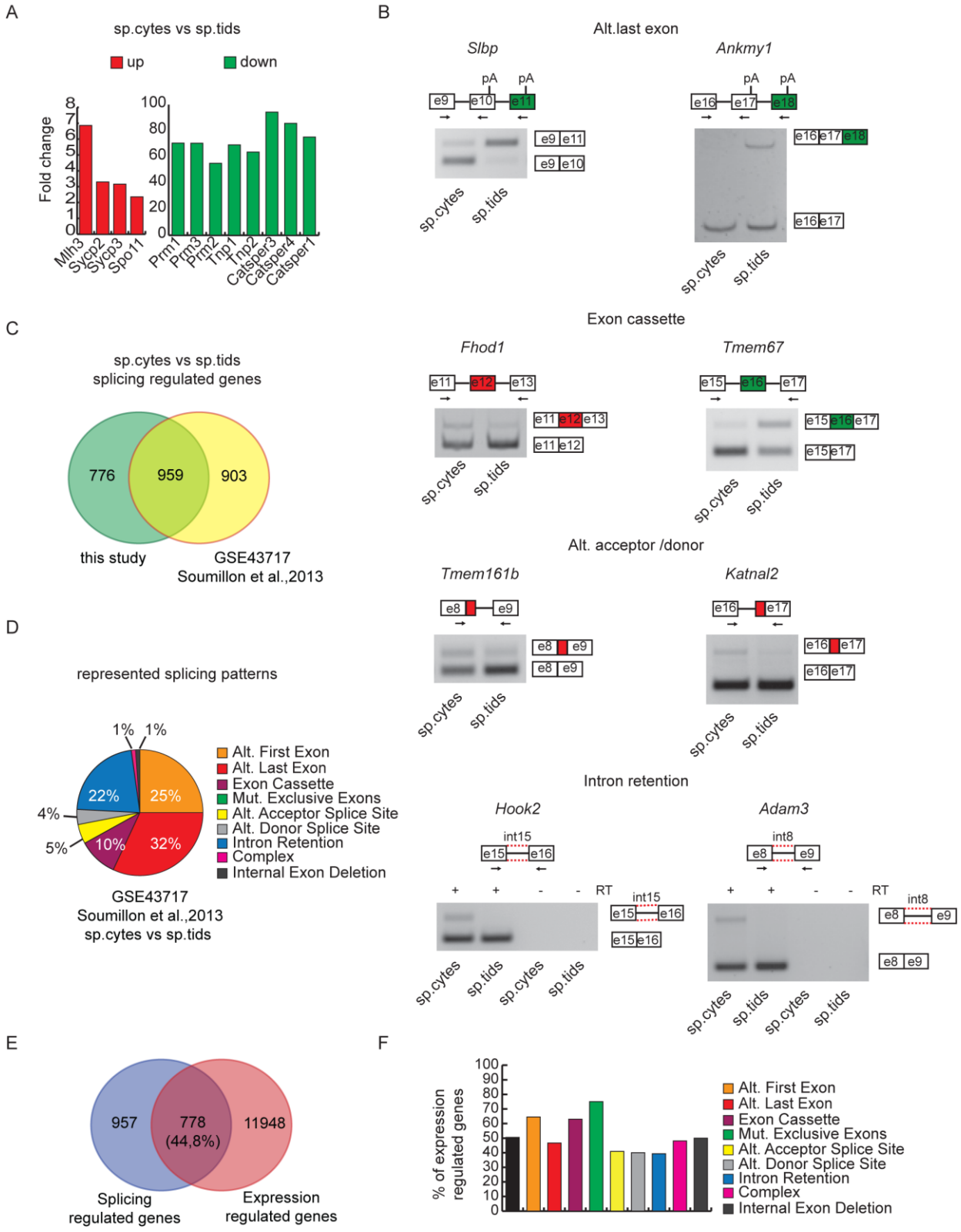

Figure S1. Analysis and validation of RNA-seq results, related to Figure 1. A) Bar graphs showing intensity of the expression fold-change between sp.cytes and sp.tids resulting from the RNA-seq analysis for indicated representative genes with known regulated expression during trans-

meiotic differentiation. B) Representative images of RT-PCR analyses for indicated AS events differentially regulated between sp.cytes and sp.tids. Red and green boxes indicate respectively up- and down-regulated events in sp.cytes compared to sp.tids. Schematic representation for each splicing event analyzed is depicted above the representative agarose or acrylamide gel. Black arrows in the scheme indicate primers used for the PCR analysis. C) Venn diagram showing overlap between groups of splicing-regulated genes between sp.cytes and sp.tids identified in this study (green circle) and by the analysis of datasets from the same cell types originated in a previous study (GSE43717, Soumillon et al., 2013) Overlap is highly significant: p-value=0; modified Fisher's test. D) Pie chart representing distribution among different splicing patterns of the regulated splicing events between sp.cytes and sp.tids revealed by analysis of GSE43717 datasets (Soumillon et al., 2013). E) Venn diagram showing percentage of overlap between group of expression- and splicing-regulated genes in sp.cytes vs sp.tids. F) Bar graph representing percentage of expression-regulated genes among the splicing regulated genes within each different splicing pattern.

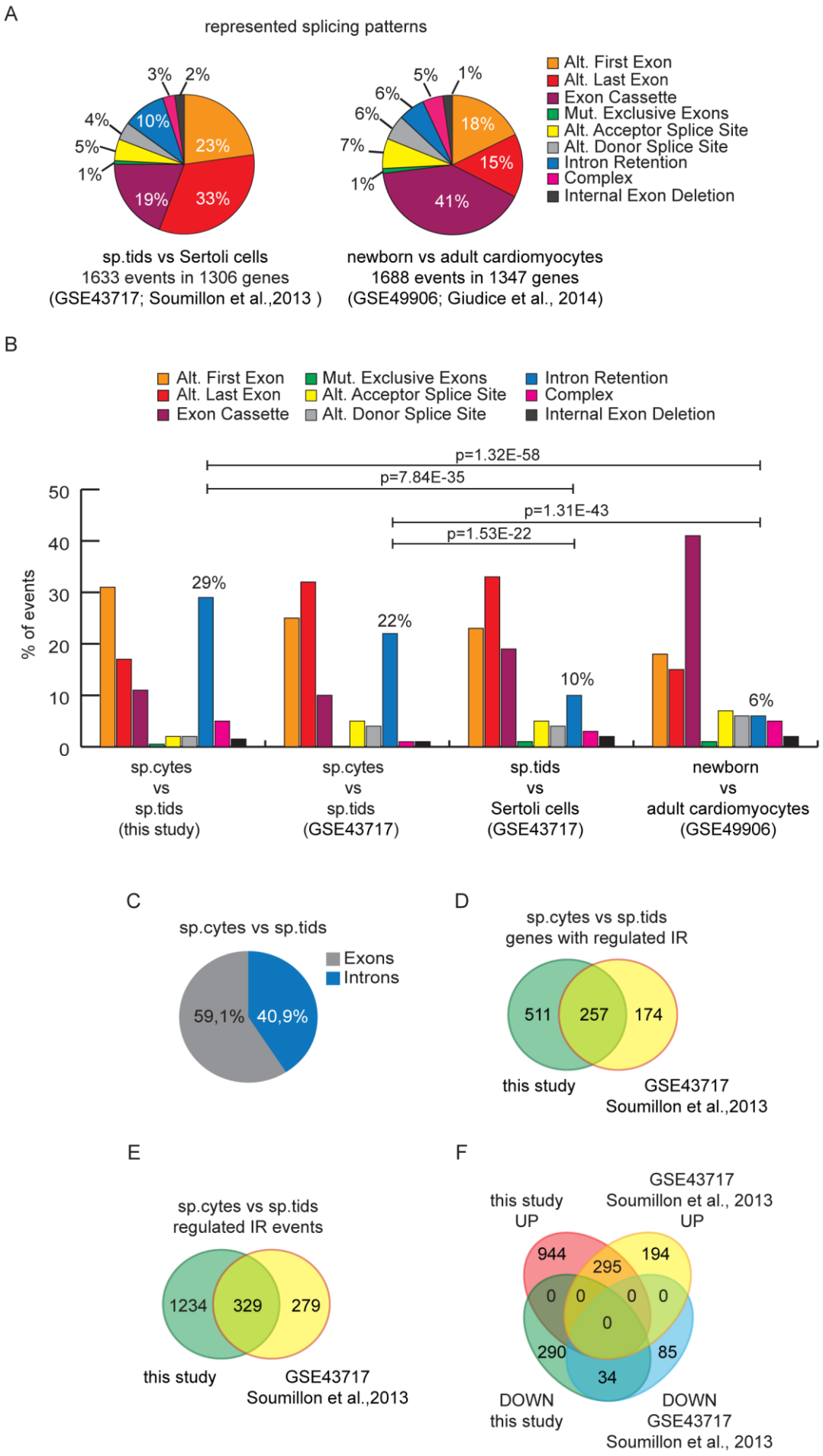
A
represented splicing patterns
3%
2%
4%
10%
5%
23%
1%
19%
33%
5%
1%
6%
6%
18%
7%
15%
1%
41%
Alt. First Exon
Alt. Last Exon
Exon Cassette
Mut. Exclusive Exons
Alt. Acceptor Splice Site
Alt. Donor Splice Site
Intron Retention
Complex
Internal Exon Deletion
sp.tids vs Sertoli cells
1633 events in 1306 genes
(GSE43717; Soumillon et al.,2013)
newborn vs adult cardiomyocytes
1688 events in 1347 genes
(GSE49906; Giudice et al., 2014)
B
Alt. First Exon
Alt. Last Exon
Exon Cassette
Mut. Exclusive Exons
Alt. Acceptor Splice Site
Alt. Donor Splice Site
Intron Retention
Complex
Internal Exon Deletion
p=1.32E-58
p=7.84E-35
p=1.31E-43
p=1.53E-22
% of events
50
40
30
20
10
0
29%
22%
10%
6%
sp.cytes vs sp.tids (this study)
sp.cytes vs sp.tids (GSE43717)
sp.tids vs Sertoli cells (GSE43717)
newborn vs adult cardiomyocytes (GSE49906)
C
sp.cytes vs sp.tids
Exons
Introns
59,1%
40,9%
D
sp.cytes vs sp.tids
genes with regulated IR
511
257
174
this study
GSE43717
Soumillon et al.,2013
E
sp.cytes vs sp.tids
regulated IR events
1234
329
279
this study
GSE43717
Soumillon et al.,2013
F
this study
UP
GSE43717
Soumillon et al., 2013
UP
944
295
194
0
0
0
0
0
290
85
34
DOWN
this study
DOWN
GSE43717
Soumillon et al., 2013

Figure S2. Intron retention features transcriptome of meiotic male germ cells, related to Figure 2. A) Pie charts representing distribution among different splicing patterns of the regulated splicing events between sp.tids and somatic Sertoli cells (left chart) and between newborn and adult cardiomyocytes (right chart) revealed by analysis of previously published RNA-seq datasets (GSE43717, Soumillon et al., 2013; GSE49906, Giudice et al., 2014). B) Analysis of RNA-seq data from both our and previously published studies revealed a significant enrichment of IR events (blue bars) in the comparison between sp. cytes and sp.tids germ cells respect to the other indicated developing/differentiation systems (p-values of Chi2 test are shown). C) Pie chart depicting proportions of exonic and intronic events among the regulated splicing events in sp.cytes compared to sp.tids. D, E) Venn diagrams showing overlap between IR genes (D) and regulated IR events (E) in sp.cytes compared to sp.tids identified in this study (green circle) and by analysis of a previous dataset (Soumillon et al., 2013). P-value = 6.97E-164 for overlap in D, p-value = 0 for overlap in E according to modified Fisher's test. F) Venn diagram showing overlap in the direction of the regulation of the IR events regulated between sp.cytes and sp.tids in this study and in analysis of Soumillon et al., 2013 dataset. P-value = 0 according to modified Fisher's test.

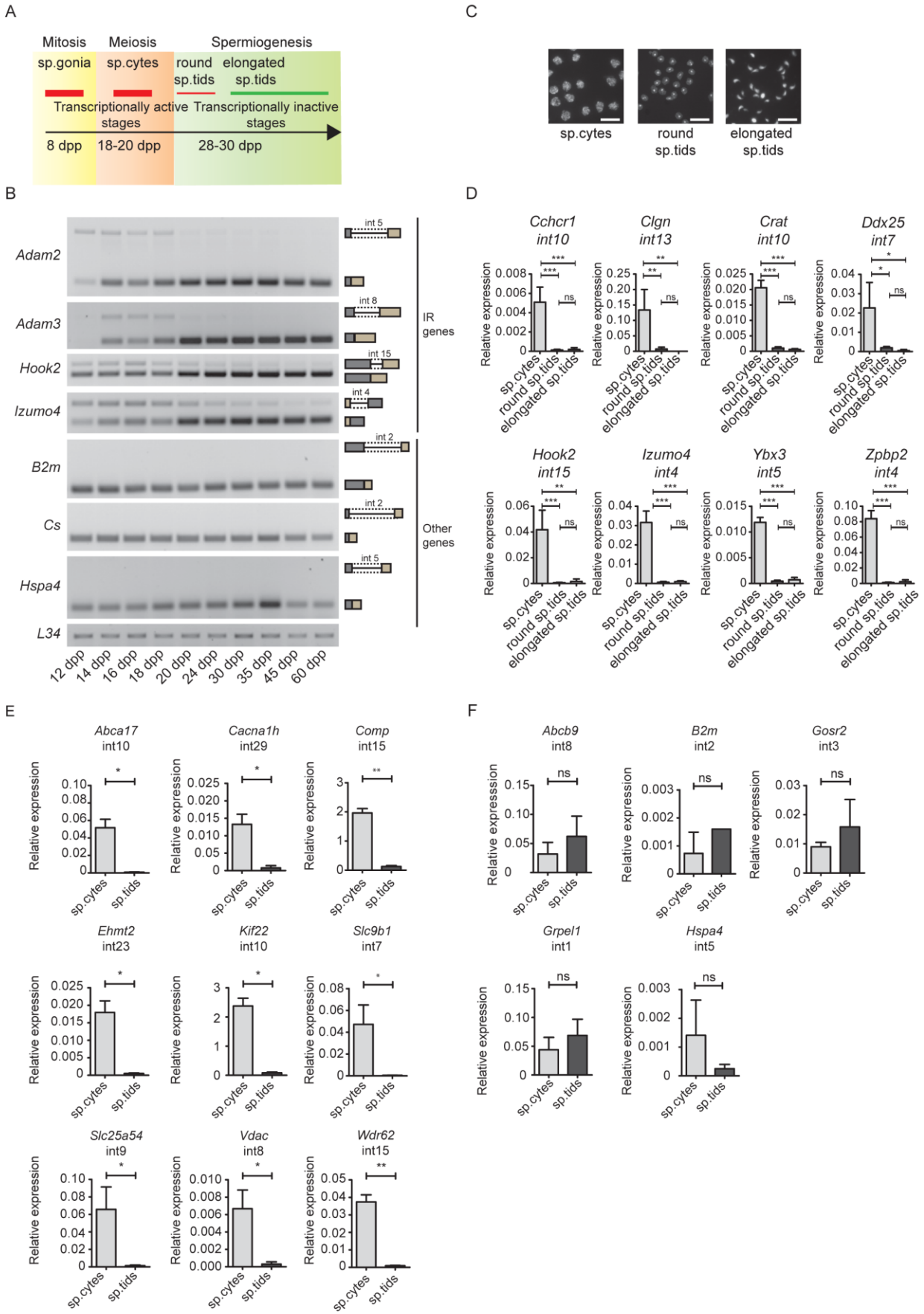
A
Mitosis
Meiosis
Spermiogenesis
sp.gonia
sp.cytes
round sp.tids
elongated sp.tids
Transcriptionally active stages
Transcriptionally inactive stages
8 dpp
18-20 dpp
28-30 dpp
C
sp.cytes
round sp.tids
elongated sp.tids
B
Adam2
Adam3
Hook2
Izumo4
B2m
Cs
Hspa4
L34
int 5
int 8
int 15
int 4
int 2
int 2
int 5
IR genes
Other genes
12 dpp
14 dpp
16 dpp
18 dpp
20 dpp
24 dpp
30 dpp
35 dpp
45 dpp
60 dpp
D
Cchcr1 int10
Clgn int13
Crat int10
Ddx25 int7
Hook2 int15
Izumo4 int4
Ybx3 int5
Zpbp2 int4
Relative expression
sp.cytes
round sp.tids
elongated sp.tids
E
Abca17 int10
Cacna1h int29
Comp int15
Ehmt2 int23
Kif22 int10
Slc9b1 int7
Slc25a54 int9
Vdac int8
Wdr62 int15
Relative expression
sp.cytes
sp.tids
F
Abcb9 int8
B2m int2
Gosr2 int3
Grpel1 int1
Hspa4 int5
Relative expression
sp.cytes
sp.tids
ns

Figure S3. Validation of intron retention events occurring in meiotic spermatocytes, related to Figure 2. A) Schematic representation of the timeline of murine spermatogenesis, its key phases and their transcriptional activity. B) Representative images of RT-PCR analyses for indicated IR-regulated and properly spliced genes in mouse testes from animals of indicated age during the first wave of spermatogenesis. Black arrows in the scheme indicate primers used for the PCR analysis. C) Representative images of Hoechst nuclear staining of purified cellular populations of meiotic pachytene spermatocytes (sp.cytes, left panel), early-stage round (middle panel) and late-stage elongated spermatids (sp.tids, right panel; scale bar 25 μm). D) Bar graphs showing results of qPCR analyses for the expression of indicated introns relative to spliced product of their flanking exons in sp.cytes, round and elongated sp.tids (mean ±SD, n=4, *p-value≤0.05; **p-value≤0.01; ***p-value≤0.001; ns=not significant - one-way ANOVA test). E,F) Bar graphs showing results of qPCR analyses for the expression of indicated introns relative to spliced product of their flanking exons in sp.cytes and round sp.tids (mean ±SD, n=3, *p-value≤0.05; **p-value≤0.01; according to two-tailed t-test; ns=not significant). Properly spliced introns of the *Abcb9, B2m, Gosr2, Grpel1*, and *Hspa4*genes were evaluated as control (F).

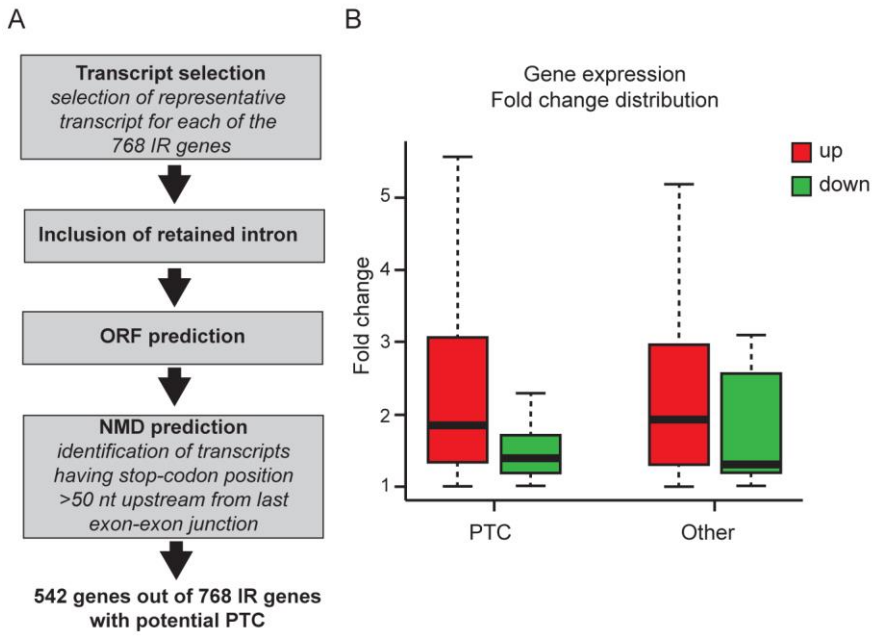

Figure S4. Meiotic IRTs are unlikely substrates for the NMD degradation pathway, related to Figure 3. A) Schematic representation of the workflow used for the identification of the IR events leading to PTC generation. B) Box plot showing distribution of fold change between spermatocytes and spermatids for genes with IR predicted (PTC) or not (other) to have PTC. No significant difference in term of expression regulation was observed between the two groups (p-value = 8.84E-1, modified Fisher's test).

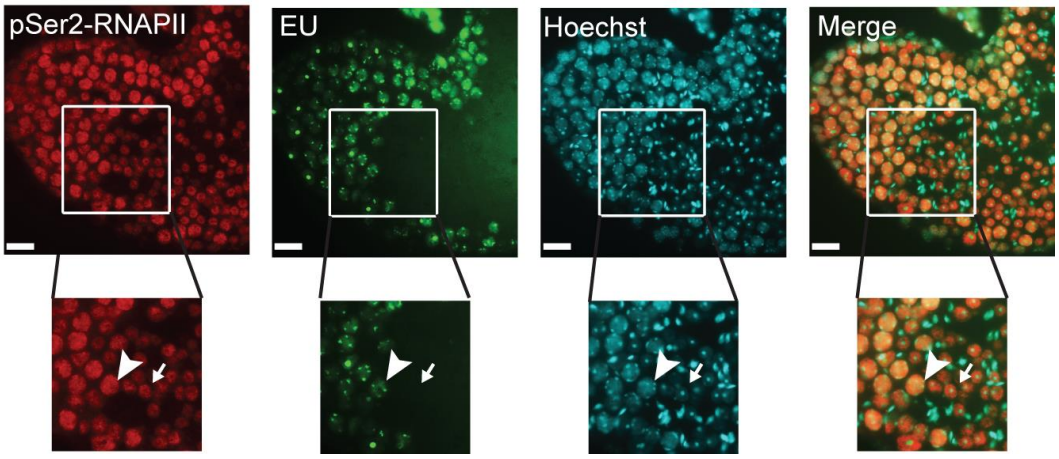

Figure S5. pSer2-RNAP II and EU-labelled RNAs mark meiotic male germ cells, related to Figure 5. pSer2-RNAPII using H5 antibody and EU-staining with Alexa488-azide of cross-sections of seminiferous tubules from adult mice cultured for 2 h 30 min in presence of EU 1mM. Hoechst staining was used to identify nuclear morphology (scale bar 25 µm). Insets show magnification of meiotic spermatocytes (arrow head) and post-meiotic round spermatids (arrow).

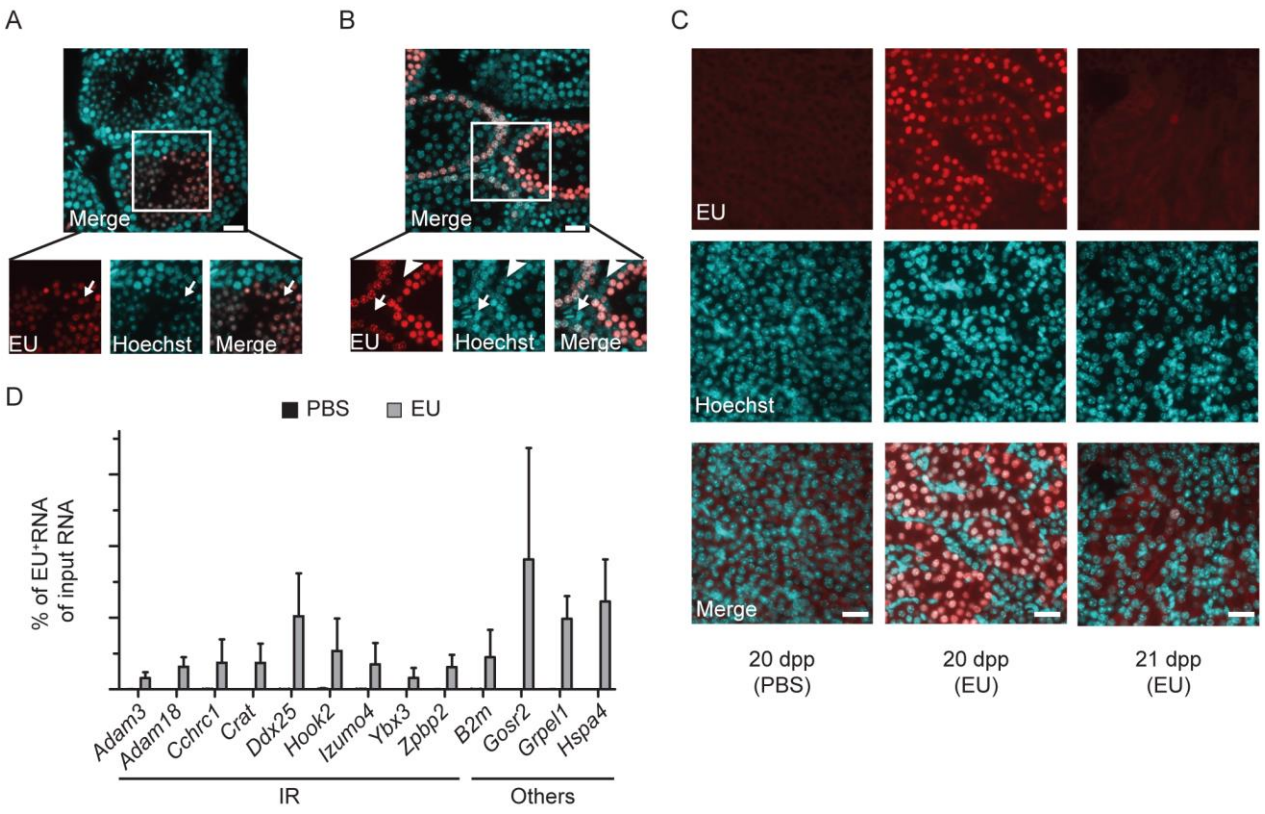

Figure S6. EU labels RNA also in kidney and with similar intensity between properly spliced and intron retaining transcripts, related to Figure 6. A,B) EU-staining with Alexa594-azide of testes paraffin-embedded cross-sections from EU- injected mice harvested at 29 dpp (A), 21 dpp (B). Hoechst nuclear staining was performed to identify nuclear morphology (scale bar 25 µm). Insets show magnification images of post-meiotic round spermatids (arrow in A), somatic Sertoli (arrow head in B) and interstitial cells (arrow in B). C) EU-staining with Alexa594-azide of kidney paraffin-embedded cross-sections of EU- and PBS (as control) injected mice, analyzed at indicated time points. Hoechst was used for nuclei staining (scale bar 25 µm). D) Bar graph showing the percentage of EU-labeled RNA pulled-down from total RNA for indicated transcripts at indicated time points estimated by qPCR analysis (mean ±SD, n=3).

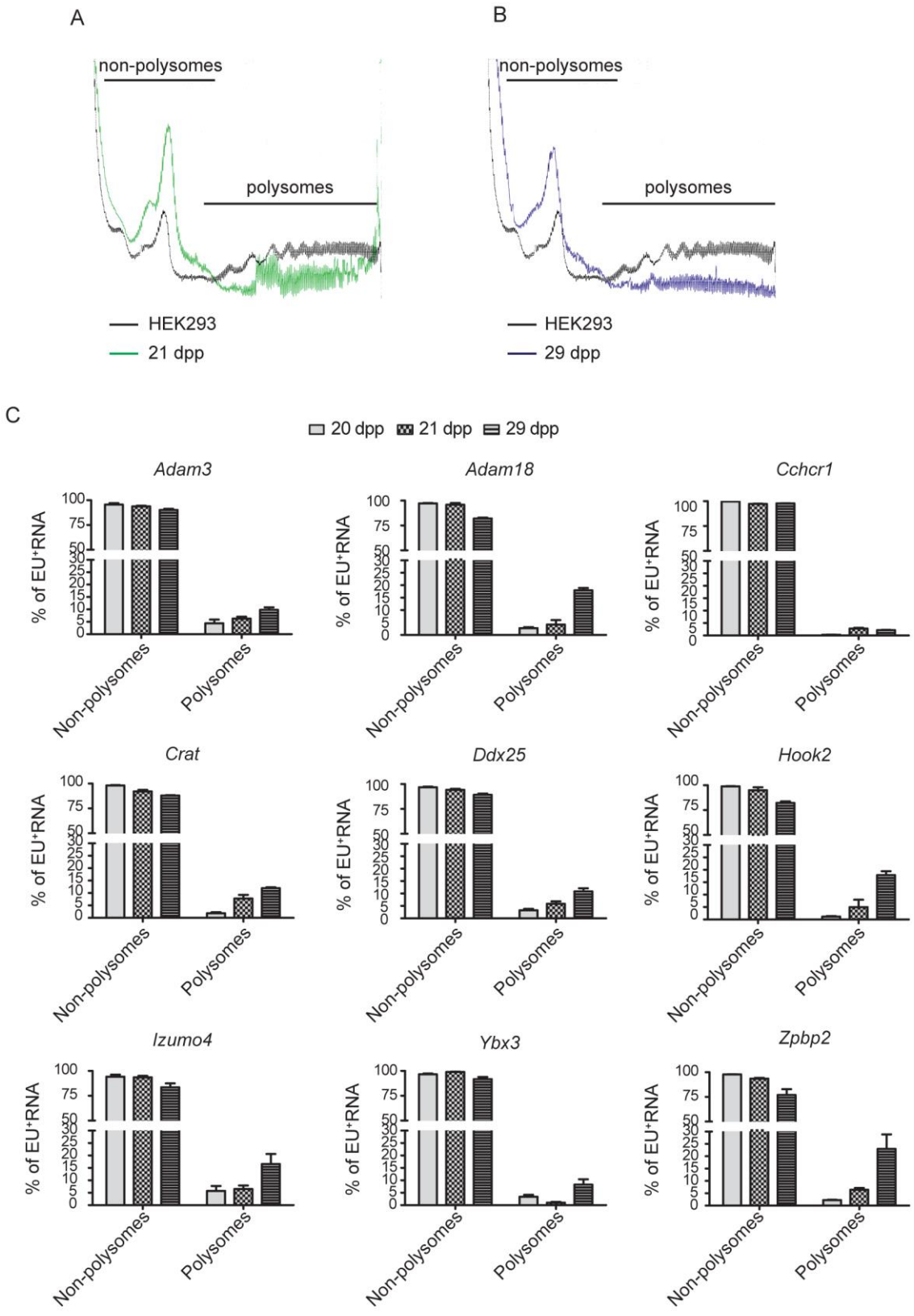

Figure S7. Related to Figure 7. RNP-polysome fractionation profile of whole testes A,B) Absorbance profile (OD = 260 nm) of sucrose gradient sedimentation of extracts from mitotic HEK293 cells (black line) and testes of 21 (green line, A) and 29 dpp mice (blue line, B). C) Bar

graph showing qPCR analysis for the distribution of EU-labeled RNAs pulled-down for indicated genes within the polysomal and non-polysomal fractions obtained from sucrose gradient fractionation of whole testes harvested at indicated time point after EU injection at 20 dpp (mean ±SD, n=3). Results are expressed as percentage of the total EU-labeled RNA captured in all fractions of the gradient.